Frontiers of Information Technology & Electronic Engineering
www.jzus.zju.edu.cn; engineering.cae.cn; www.springerlink.com
ISSN 2095-9184 (print); ISSN 2095-9230 (online)
E-mail: jzus@zju.edu.cn

Review:

XL-MIMO channel measurement, characterization, and modeling for 6G: a survey*

Pan TANG†1, Jianhua ZHANG†‡2, Haiyang MIAO2, Qi WEI2, Weirang ZUO2, Lei TIAN2, Tao JIANG3, Guangyi LIU3

[1]*School of Electronic Engineering, Beijing University of Posts and Telecommunications, Beijing 100876, China*

[2]*School of Information and Communication Engineering, Beijing University of Posts and Telecommunications, Beijing 100876, China*

[3]*China Mobile Research Institute, Beijing 100053, China*

†E-mail: tangpan27@bupt.edu.cn; jhzhang@bupt.edu.cn

Received Mar. 1, 2024; Revision accepted June 18, 2024; Crosschecked Sept. 19, 2024; Published online Nov. 5, 2024

Abstract: Extremely-large-scale multiple-input multiple-output (XL-MIMO) technology, offering vast spatial degrees of freedom by deploying a huge number of antennas, is a promising enabling technology to empower sixth-generation mobile networks (6G). The XL-MIMO channel model is a prerequisite of XL-MIMO technology optimization, system design, and performance evaluation. In this paper, we provide an overview of challenges and ongoing research in XL-MIMO channel measurement, characterization, and modeling. In particular, characterizing and modeling near-field effects and spatial non-stationarity (SnS) are discussed. Also, the channel modeling methods that can describe these new channel characteristics are surveyed. Furthermore, open issues in XL-MIMO channel measurement, characterization, and modeling are presented to give insights into future XL-MIMO channel research.

Key words: 6G; XL-MIMO; Near-field; Channel measurement; Channel modeling
https://doi.org/10.1631/FITEE.2400140 **CLC number:** TN929.5

1 Introduction

International Telecommunication Union-Radiocommunication Sector (ITU-R) Working Party (WP) 5D agreed to the draft new recommendation "Framework and Overall Objectives of the Future Development of IMT for 2030 and Beyond" in June 2023 and published it as ITU-R M.2160 in December 2023 (ITU-R, 2023). This recommendation identifies 6 usage scenarios and 15 capabilities for sixth-generation mobile networks (6G) technologies derived from existing fifth-generation mobile networks (5G) systems. For example, 6G is expected to provide evolving and new capabilities compared to 5G, such as a larger peak data rate and user-experienced data rates, positioning, sensing-related capabilities, and coverage. Based on these capabilities, 6G is envisaged to enable new usage scenarios, e.g., immersive communication, ubiquitous connectivity, and integrated sensing and communication (ISAC). To successfully evolve on the way to 6G, some promising technologies are proposed as enablers, e.g., extreme multiple-input multiple-output (E-MIMO), terahertz (THz) communication, reconfigurable intelligent surface (RIS) (Liu YW et al., 2023), and the digital twin network (DTN) (Zhang JH et al., 2023). Among them, E-MIMO is an umbrella term for a range of extensions of massive MIMO in different trends, such as extremely-large-scale MIMO (XL-MIMO)

‡ Corresponding author
* Project supported by the National Natural Science Foundation of China (Nos. 62201086, 62101069, and 92167202), the National Science Fund for Distinguished Young Scholars (No. 61925102), and the BUPT-CMCC Joint Innovation Center
ORCID: Pan TANG, https://orcid.org/0000-0003-0432-7361; Jianhua ZHANG, https://orcid.org/0000-0003-0484-6188

(Yang B et al., 2023), RIS-based massive MIMO (Zhao et al., 2024), and artificial intelligence (AI) assisted massive MIMO. E-MIMO is expected to achieve better spectrum efficiency, larger network coverage, more accurate positioning, more accurate sensing, higher energy efficiency, and so on (ITU-R, 2023).

XL-MIMO can be regarded as the further extension of 5G massive MIMO to a higher spatial dimension, i.e., using hundreds or even thousands of antennas at the base station (BS) (Huo et al., 2023). It is worth noting that XL-MIMO can be deployed with traditional antenna arrays, distributed antennas, RISs, and holographic antennas (Wei et al., 2022; Yang SJ et al., 2023; Gong et al., 2024). Because RIS and holographic communications are not considered in the current Third-Generation Partnership Project (3GPP) standardization work, this paper considers only XL-MIMO deployed with traditional antenna arrays. As a result of the deeper use of space resources, XL-MIMO can significantly increase system capacity and spectrum efficiency (Zhi et al., 2024). For example, in Saad et al. (2020), XL-MIMO was expected to accomplish a 10-fold increase in the spectral efficiency for 6G. However, as the number of antennas increases, the boundary between the near and far fields expands, and users will be more likely located in the near field. This would violate the far-filed assumption and consequently bring challenges to channel modeling and performance analysis (Cui et al., 2023; Liu MY et al., 2024).

The channel is the medium between the transmitter (Tx) and receiver (Rx) in wireless communications. Its properties determine the performance limit of wireless communication systems (Molisch, 2011). A channel model is a mathematical description of the effects of a communication channel through which wireless signals are propagated. To better design and evaluate XL-MIMO communication systems, a fundamental understanding of XL-MIMO channel properties and a practicable XL-MIMO channel model are extremely crucial (Zhang JH et al., 2023). As shown in Fig. 1, except for the spatial non-stationarity (SnS) inherited from massive MIMO channels, new channel characteristics, e.g., spherical wave and visible region (VR), simultaneously arise in XL-MIMO channels (Li MT et al., 2023). This means that due to the extension of antenna arrays in the spatial domain, different parts of the antenna array at the BS would see different propagation environments, i.e., scatterers. For example, users located in different positions would have different views of scatterers when scatterers are within the near field of the user or there are obstacles between scatterers and the user. Moreover, on a much smaller scale of observation, the radio wave can no longer be reduced to a plane wave, but rather a spherical wave (Yuan ZQ et al., 2023a). Subsequently, the distances and incident wave directions between the Tx and Rx antenna elements vary over the antenna array. In

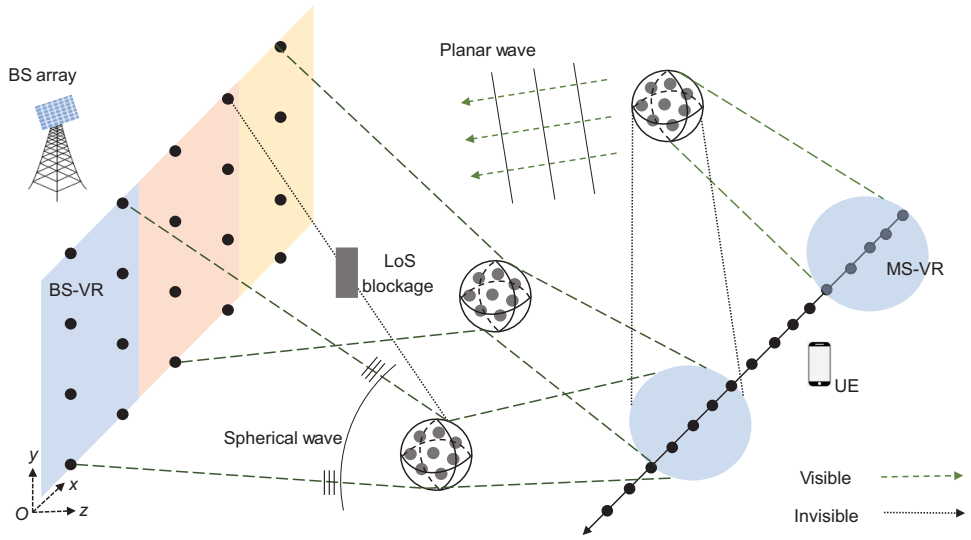

Fig. 1 Near-field propagation with SnS and VR of the cluster (SnS: spatial non-stationarity; VR: visible region; BS: base station; MS: mobile station; UE: user equipment; LoS: line of sight)

general, plane wave and spatial stationarity assumptions no longer hold. Accordingly, challenges are brought to XL-MIMO channel measurements and modeling in terms of building channel sounders, estimating channel parameters, characterizing channel properties, and proposing new modeling theories and structures. The challenges are discussed in detail later.

There has been some research on XL-MIMO channel measurement and modeling. For example, Zheng et al. (2023) conducted channel measurements in urban scenarios using different types of antennas and proposed a general three-dimensional (3D) non-stationary geometry based stochastic model (GBSM) suitable for 6G massive MIMO. In Yuan ZQ et al. (2023a), channel measurements were conducted by using a large-scale virtual uniform circular array, and a low-complexity SnS channel modeling framework was proposed. This model, characterized by its low complexity, is suitable for link- and system-level evaluation of XL-MIMO antenna systems. In terms of channel model standardization, 5G channel model standards, i.e., ITU-R M.2412 and 3GPP technical report (TR) 38.901, can support the simulation of massive MIMO channels, but not the simulation of XL-MIMO channels. Therefore, 3GPP recently approved a study item (SI) for release 19 to study channel models for 7–24 GHz in the radio access network (RAN) 102 meeting in Dec. 11–15, 2023. Specifically, one objective of this SI is to extend the 5G TR 38.901 channel model to support the modeling of near-field effects and SnS. Immediately afterward, it is urgent to study XL-MIMO channel characteristics and modeling methods based on abundant channel measurements. A review of XL-MIMO channel measurements and models is helpful to know the current research progress and obtain insights into future work.

Until now, there have been some surveys of massive MIMO (de Figueiredo, 2022; Dala Pegorara Souto et al., 2023), including massive MIMO channel measurements and models, but not XL-MIMO channel measurements and models (Wang CX et al., 2018; Zhang P et al., 2018; de Figueiredo, 2022). In light of this status, this paper aims to give a comprehensive survey to review the current research progress in XL-MIMO channel measurements and models. Also, challenges and future research directions are discussed.

The contributions of this paper are summarized as follows:

1. This paper gives a survey of the current research progress in XL-MIMO channel measurements, including channel measurement methods and parameter extraction methods.

2. Recent research on the XL-MIMO channel characteristics, including near-field effects, SnS characteristics, channel capacity, and channel hardening, are reviewed.

3. In terms of XL-MIMO channel modeling methods, statistical channel models, deterministic channel models, and hybrid channel models are surveyed. Specifically, the 3GPP-like channel modeling method is discussed.

4. Future research directions are presented in terms of channel measurement, characterization, and modeling, giving insights into future XL-MIMO channel research.

2 XL-MIMO channel measurements and characterization

Channel measurements and characterization are the basis for XL-MIMO channel characteristic analysis and modeling. Through abundant channel measurements in typical communication scenarios, channel impulse responses (CIRs) that represent propagation characteristics in the scenarios can be obtained. Subsequently, channel parameter extraction algorithms are used to characterize channels based on measurement CIRs. As the scale of the antenna array increases, the XL-MIMO channel will have some characteristics that are different from those of traditional channels, such as a spherical wavefront and non-stationarity. These bring challenges to correctly measuring and extracting these characteristics. In this section, we first discuss the challenges and then review the current progress of channel measurement methods and channel parameter extraction algorithms for XL-MIMO communications, as shown in Table 1. Detailed discussions are given below.

2.1 Channel measurement methods

2.1.1 Challenges

To accurately obtain CIRs in real communication scenarios, the channel sounder should have at least the same or even better radio frequency (RF)

Table 1 Recent progress in XL-MIMO channel measurements

	Scenario	Antenna and number of elements	Carrier frequency (GHz)	Parameter extraction algorithm	Channel characteristics	Reference
Indoor	Lecture hall	Virtual UPA, 144	5.6	NM	SnS: DS, condition number, etc.	Li JX and Zhao, 2014
	Stadium	Virtual ULA, 128	1.47/4.45	NM	SnS: channel envelope coefficient, rice K-factor, DS, etc.	Liu L et al., 2015
	Office	Virtual URA, 2601/5776/ 8281/14 641	11/16/28/38	SAGE	Spherical wavefront, SnS: cluster birth-death, DS, AS, channel capacity, etc.	Huang J et al., 2017
	Theater	Virtual UPA, 256	11	SAGE	PL, SF, SnS: DS, etc.	Li JZ et al., 2017
	Theater	Virtual UPA, 256	11	SAGE	SnS: MPC birth-death, AS, etc.	Li JZ et al., 2018b
	Lobby	Virtual UPA, 256	11	SAGE	SnS: MPC power, spherical wavefront, etc.	Li JZ et al., 2018a
	Laboratory	Virtual UPA, 441	28	SAGE	RMS DS, AS, SnS: number of MPCs, etc.	Mudonhi et al., 2020
	Room	Virtual uniform circular array, 720	26.5–32.5	NM	SnS: spherical wavefront, etc.	Yuan ZQ et al., 2023b
	Meeting room	Virtual UPA, 1800	26–30	NM	Near-field: CIR, PADP, etc.	Mbugua et al., 2024
Outdoor	Court yard	Virtual LA, 128	2.6	SAGE	SnS: rice K-factor, etc.	Payami and Tufvesson, 2012
	Campus	Virtual ULA/uniform cylindrical array, 128	2.6	NM	SnS: PAS, etc.	Gao X et al., 2012
	UMa	Virtual UPA, 256	3.5	SAGE	PDP, PAS, etc.	Yu et al., 2016
	UMa	Virtual UPA, 256	3.5	SAGE	PAS, SnS: VR, etc.	Wang C et al., 2017
	Top of building	Virtual UPA, 1600	15	SAGE	Rice K-factor, RMS DS, AS, SnS, etc.	Chen JJ et al., 2017
	UMa/UMi	Virtual UPA, 256	3.5/6	SAGE	PAS, RMS AS, channel capacity, etc.	Zhang JH et al., 2018
	UMi	URA, 128	142	NM	PAS, RMS AS, etc.	Ju and Rappaport, 2021
	Urban	ULA/DULA, 128	5.3	SAGE	Non-stationarity: RMS DS, RMS AS, spherical wavefront, channel capacity, etc.	Zheng et al., 2023
	O2I	Virtual UPA, 256	3.5	NM	DS	Xu et al., 2017

AS: angular spread; CIR: channel impulse response; DS: delay spread; DULA: distributed uniform linear array; LA: linear array; MPCs: multipath components; NM: not mentioned; O2I: outdoor-to-indoor; PADP: power angle delay profile; PAS: power angular spectrum; PDP: power delay profile; PL: path loss; RMS: root-mean-square; SAGE: space-alternating generalized expectation–maximization; SF: shadow fading; SnS: spatial non-stationarity; ULA: uniform linear array; UMa: urban macrocell; UMi: urban microcell; UPA: uniform planar array; URA: uniform rectangular array; VR: visible region

specifications, e.g., bandwidth and antenna number. Because XL-MIMO communications would deploy hundreds, even thousands, of antenna elements, the XL-MIMO channel sounder should deploy as many antenna elements to assume high resolution in the spatial domain. However, it is extremely expensive to build hundreds or thousands of RF channels to drive each antenna element. A time-division multiplexing (TDM) based MIMO channel sounder is an effective solution for reducing cost, and can use one RF channel to drive a large number of antenna elements at different time slots. Nonetheless, measuring a round of sub-channels would be time-consuming. In particular, it is challenging to complete a round of sub-channel measurements within coherence time in environments with high mobility. Next, some progress that addresses these challenges is reviewed.

2.1.2 Progress

There are mainly two ways to build antenna arrays in XL-MIMO channel sounders. One is to use a real antenna array (RAA) with XL antenna elements, as shown in Fig. 2a. RAA is usually paired with a time-domain measurement system based on sliding correlation, as the block diagram shows in Fig. 3. Mux in the diagram is a high-speed electronic switch, which can complete a round of sub-channel switching within the channel coherence time, thereby realizing the TDM working mode. The arbitrary waveform generator of the Tx generates a baseband spread spectrum pseudo-random signal. The local oscillator moves the signal to the target frequency for transmission through up-conversion. After receiving the signal, the Rx down-converts the frequency to the baseband and stores it in the disk after analog-to-digital conversion. During data processing, the autocorrelation characteristics of pseudo-random sequences are used to obtain the CIRs. The time-domain measurement system has separate transmitting and receiving ends, which can cover a larger measurement range, and uses a high-precision rubidium clock or Global Positioning System (GPS) module to provide clock signals to achieve synchronization between sub-channels. This method can directly measure the XL-MIMO sub-channels. However, the manufacturing cost of this kind of antenna array is very high, and it cannot be easily moved due to its large size, especially in sub-6 GHz bands with large wavelengths. In addition, it is difficult to measure the pattern of the large antenna

array in a microwave anechoic chamber, which is a prerequisite to extracting channel parameters from measurement data. Therefore, RAA is rarely used in XL-MIMO channel measurement campaigns.

Another method of building XL-MIMO is to use virtual antenna arrays (VAAs). For example, the virtual array can be formed by moving a single antenna or a small-scale antenna array in the spatial domain, as shown in Figs. 2b and 2c, respectively. VAA formed by a small array is usually used with the time-domain measurement system shown in Fig. 3. The VAA formed by a single antenna can be used with either a time-domain measurement system or a frequency-domain measurement system (Fig. 4). The core of the frequency-domain measurement system is a vector network analyzer (VNA). The transmitting and receiving antennas are connected to it through cables, and the channel frequency response (CFR) within a frequency band is obtained through frequency sweeping. By using low-loss optical fibers, the measurement distance of frequency-domain measurement systems can be greatly extended (Lyu et al., 2021). This method needs only a mechanical 3D turntable and a single antenna or a small-scale antenna array, so that it is relatively cost-efficient and easy to operate. Therefore, VAA is more commonly used in measurement campaigns (Li JZ et al., 2017; Zhang JH et al., 2018; Yuan ZQ et al., 2023a). However, moving operations are time-consuming and the static condition in a measurement environment should be guaranteed. Or, the statistical properties of sub-channels in different measurement time slots may be different, which makes the channel parameter extraction algorithms invalid.

2.1.3 Summary

Because it is extremely costly to equip each antenna with an RF channel, most XL-MIMO channel measurements adopt the TDM operating mode, using one RF channel to drive different array elements in different time slots. There are currently

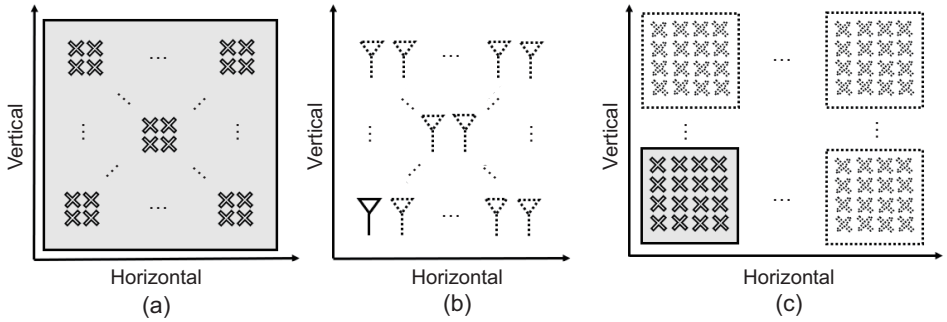

Fig. 2 XL-MIMO array configuration: (a) RAA; (b) VAA formed by a single antenna; (c) VAA formed by a small array (RAA: real antenna array; VAA: virtual antenna array)

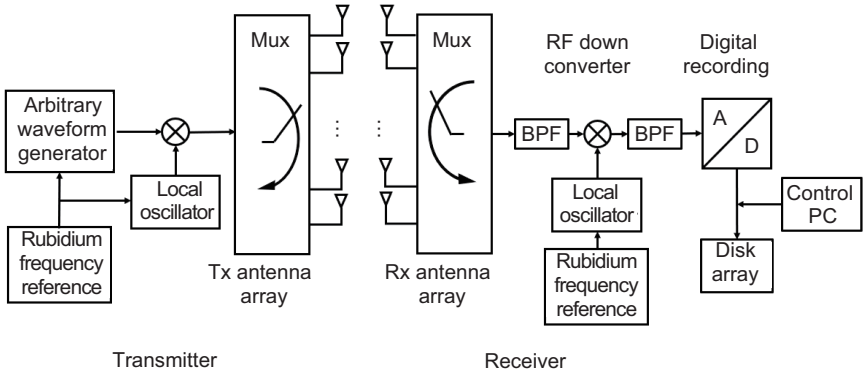

Fig. 3 Block diagram of RAA applied to a time-domain XL-MIMO measurement system (RAA: real antenna array; BPF: bandpass filter; PC: personal computer; RF: radio frequency). Reprinted from Miao et al. (2024), Copyright 2024, with permission from IEEE

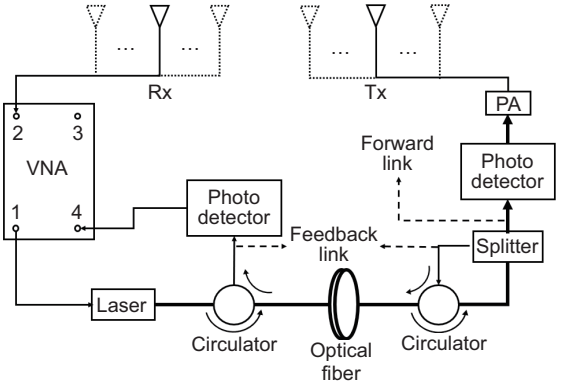

Fig. 4 Block diagram of VAA applied to a frequency-domain XL-MIMO measurement system (VAA: virtual antenna array; VNA: vector network analyzer; PA: power amplifier). Reprinted from Yuan ZQ et al. (2023a), Copyright 2023, with permission from IEEE

two main forms of XL arrays that support this working mode. The first is to use RAA, combined with high-speed electronic switches, to complete a round of data collection within the channel coherence time. This method has high acquisition speed, but the antenna array is large, the cost is high, and it is difficult to obtain the antenna pattern. The other is to use a single antenna or small array with a 3D mechanical turntable to form a VAA. This method is simple to operate and low in cost, but the acquisition time is relatively long. It is difficult to cope with many of the dynamic application scenarios of 6G. In addition, the phase sensitivity of large array antennas should be considered. Exploring a dynamic and high-performance channel detection system is worthy of further study.

2.2 Parameter extraction methods

2.2.1 Challenges

The accuracy of the channel model relies on an accurate characterization of the distribution of relevant channel parameters. Therefore, it is necessary to use accurate and computationally efficient signal processing tools to extract channel parameters from measurement data. In traditional channel parameter estimation algorithms, it is commonly assumed that the distance between scatterers and the antenna array is much greater than the size of the antenna array, and the radio wave is considered planar. However, in the case of XL-MIMO channels, as the size of the antenna array increases, the far-field assumption may be violated and the radio wave is a spherical wavefront. This brings challenges to traditional channel parameter estimation algorithms that assume a planar wavefront.

2.2.2 Progress

The existing channel parameter estimation algorithms can be classified mainly into three categories: beamforming algorithms, parametric subspace based estimation (PSBE) algorithms, and maximum likelihood estimation (MLE) based algorithms. The algorithms included in these three categories are shown in Table 2.

Table 2 XL-MIMO channel parameter estimation algorithms

Category	Algorithm	Reference
Beamforming		
PSBE	MUSIC	Schmidt, 1986; Saleh and Valenzuela, 1987
	ESPRIT	Fayad et al., 2015
MLE-based	EM	Regier and Moodie, 2016
	SAGE	Fleury et al., 2002
	RiMAX	Gaillot et al., 2011

EM: expectation–maximization; ESPRIT: estimation of signal parameters via the rotational invariance techniques; MLE: maximum likelihood estimation; MUSIC: multiple signal classification; PSBE: parametric subspace based estimation; RiMAX: Richter's maximum likelihood estimation; SAGE: space-alternating generalized expectation–maximization

The classical beamforming algorithm estimates the multipath angle information by forming the spatial spectrum through weighted vectors, which is robust and computationally efficient. However, its spatial resolution is low, which limits its application in XL-MIMO channels. Furthermore, the plane wave assumption is typically used so that the array complex weight vector is determined only from the beam-steering direction. The main PSBE algorithms are the multiple signal classification (MUSIC) algorithms (Schmidt, 1986; Saleh and Valenzuela, 1987) and the estimation of signal parameters via the rotational invariance techniques (ESPRIT) algorithm (Fayad et al., 2015), which are two techniques that perform joint estimation of delay angles usually under the plane wave and narrowband assumptions. For XL-MIMO channel scenarios with severe near-field effects, the near-field MUSIC algorithm, which can simultaneously estimate the direction of the source and its distance to the reference array

element, was proposed in Huang YD and Barkat (1991) and He J et al. (2012). As compared with the far-field MUSIC algorithm, the computational complexity of the near-field MUSIC algorithm is too high, and the hardware requirements are higher.

MLE-based algorithms include mainly the space-alternating generalized expectation–maximization (SAGE) algorithm (Fleury et al., 2002) and Richter's maximum likelihood estimation (RiMAX) algorithm (Gaillot et al., 2011), in which the SAGE algorithm is an extension of the expectation–maximization (EM) algorithm (Regier and Moodie, 2016). Both algorithms solve the channel parameters by maximizing the likelihood function; the difference is that the EM algorithm needs to update all the parameters in each iteration. Hence, the EM algorithm is more complex. The SAGE algorithm divides the parameters into subsets to be updated in alternating iterations, which improves the algorithm's computational efficiency and convergence speed. These algorithms have a higher computational resolution but are not computationally efficient because the search process is iterative. To satisfy the premise of spatial alternation, this type of algorithm is implemented under a narrowband assumption with plane waves, which prevents its application to large-scale arrays.

To solve the problem of inaccurate estimation due to the near-field effect of XL-MIMO, Chen JJ et al. (2016b) proposed a signal model based on a spherical wavefront. Using real channel measurement data and the azimuth of arrival (AoA) delay power spectra (PS) of the original CIRs calculated by using the Bartlett beamforming method, the reconstructed CIRs and the residuals are computed, respectively. The results show that the residual PS computed using the spherical wave model is 10 dB lower than that obtained from the plane wave model, which proves that better performance can be obtained under the assumption of a spherical wavefront. Hong et al. (2023) proposed a geometrically assisted SAGE (GA-SAGE) algorithm, which is based on a spherical wavefront multipath model, provides joint channel estimation and scatterer localization, and is capable of reproducing spatial consistency and SnS phenomena. The algorithm is verified by real measurements to be superior to the traditional SAGE algorithm in terms of multipath component (MPC) estimation accuracy, likelihood convergence speed, and computational cost. In Zhou et al. (2023), a new SAGE algorithm was proposed for parameter estimates of wideband SnS wireless channels to antenna polarization (SAGE-WSNSAP). This algorithm adds SnS by introducing birth-death coefficients at Tx and Rx sides into the parametric model. The power extraction ratios of the three algorithms, far-field SAGE, near-field SAGE, and SAGE-WSNSAP, for the measurement CTFs are also compared, which are 64%, 66%, and 70% for line of sight (LoS) scenarios, and 46%, 49%, and 56% for non-line of sight (NLoS) scenarios, respectively, which verifies that the estimates of the proposed algorithms have a higher similarity to the measurements. Yuan ZQ et al. (2023a) proposed a generalized phase mode selection criterion to guide the implementation of a frequency-invariant beamformer (FIBF) in broadband 3D near-field millimeter-wave (mmWave) scenarios, which can accurately characterize uniform circular array based mmWave channels. In Yuan ZQ et al. (2023b), the influence of near-field effects on phase mode selection was analyzed, expressing the m^{th}-order manifold $\hat{a}_m(f,\Theta_k)$ as the summation of a series of Bessel functions:

$$\begin{aligned}\hat{a}_m\left(f,\Theta_k\right)=&\mathrm{e}^{\mathrm{j}m\phi_k}G_m(f)\sum_{l=-L}^{L}\left[B_l\left(f,r,d_k,\theta_k\right)\right.\\&\left.\cdot\mathrm{j}^{m+l}J_{m+l}\left(wr\sin\theta_k\right)\right],\end{aligned}\tag{1}$$

where B_l are the coefficients of the Fourier series, dependent on $\{f,r,d_k,\theta_k\}$. L denotes the series order. Generally, a smaller d_k results in a larger L. In far-field scenarios, $L=0$ holds. Due to the property $J_n(x)\approx 0$ for $n>x$, some high-order (i.e., high m) phase modes suffer from weight drop as $m+l$ exceeds $wr\sin\theta_k$, while the low-order phase modes retain the same normalized power in the transformation from the far field to the near field. Hence, the high-order phase modes are biased due to the near-field conditions, where the weight drop results in power loss of the beam pattern. A generic mode-selection guideline is proposed to guide the implementation of an FIBF in broadband 3D near-field mmWave scenarios, using three sets of real-world data with different frequencies (15, 28, and 29 GHz with 2 GHz bandwidth) and radii (0.5 m and 0.24 m) of measurement data to verify the validity and generality of the criterion, which proves that the criterion can accurately characterize the uniform circular array based mmWave channel.

2.2.3 Summary

In XL-MIMO systems, the significant increase in the antenna array size may cause the assumption of the planar wavefront signal model in traditional estimation algorithms to be invalid, which in turn leads to inaccurate parameter estimation results. To address this challenge, the existing MLE-based scheme is to introduce a spherical wave model for estimation based on traditional algorithms, but this will increase the computational cost. Meanwhile, there are fewer studies on parameter estimation algorithms for channels with SnS effects, and further work is needed.

2.3 Channel characterization

2.3.1 Challenges

As the antenna size of XL-MIMO increases, the Rayleigh distance of the array also increases, which may lead to the Rayleigh distance of the BS antenna array in a typical deployment scenario of 6G being larger than the distance between the BS and the user. In this case, the electromagnetic wave arrives at a spherical wavefront, which no longer meets the planar wavefront assumption in the traditional model, and at the same time, the observed channels of the different elements on the array may be different, and there is an SnS phenomenon in the array domain. The characterization of the spherical wavefront and SnS phenomenon is a new challenge introduced in the XL-MIMO channel. To explore the changing law of XL-MIMO channel characteristics from far to near field, it must be possible to accurately characterize these channel properties, which provides a theoretical basis for the modeling of XL-MIMO channel.

It has been theoretically proven that XL-MIMO has the potential to significantly improve performance in terms of link reliability, spectral efficiency, and transmission energy efficiency (Ngo et al., 2013; Rusek et al., 2013). However, the attractive features of XL-MIMO are based on optimistic assumptions about propagation conditions. So far, research has been based mainly on theoretical independent and identically distributed (i.i.d.) complex Gaussian (i.e., Rayleigh fading) channels and an unlimited growth of the number of antennas. Under which channel conditions XL-MIMO can have better performance in actual mobile communications has been a matter of concern and research.

2.3.2 Progress

Some XL-MIMO channel measurements have been conducted to investigate the above-mentioned new characteristics. In the following, recent advances in the study of SnS, spherical wave effects, channel capacity, and channel hardening in XL-MIMO channels are reviewed.

1. Spatial non-stationarity

SnS has been observed in several XL-MIMO channel measurement campaigns. Payami and Tufvesson (2012) and Chen JJ et al. (2016a) investigated the variation in channel gains on the array domain. The channel gains P can be calculated from CIR $h(\tau)$ as $P=\left|\int h(\tau)\mathrm{d}\tau\right|$; these studies observed that channel gains exhibit random variations in the array, with no clear deterministic trend. Payami and Tufvesson (2012) and Chen JJ et al. (2016a, 2017) investigated the variation of the K-factor on the array domain. Observations indicate that the K-factor at different positions on the array fluctuates within the $[-8, 8]$ dB range. Its variation pattern is scene-dependent, with more pronounced changes observed in the horizontal dimension in indoor hall environments, whereas in outdoor scenarios, the K-factor exhibits more significant variations in the vertical dimension.

In Gao X et al. (2012, 2015), Payami and Tufvesson (2012), Huang J et al. (2017), Li JZ et al. (2018a), Yuan ZQ et al. (2023a), and Mbugua et al. (2024), the SnS phenomena were observed from the power delay and power angle spectrum perspectives. As shown in Fig. 5, the S-shaped distribution of the MPCs reflects the presence of spherical wave phenomena, and the fact that some MPCs are visible on some of the arrays reflects the presence of SnS. Huang J et al. (2017) and Mbugua et al. (2024) specifically analyzed the variations in the power delay spectrum on the array domain, whereas Payami and Tufvesson (2012), Gao X et al. (2012, 2015), and Li JZ et al. (2018a) examined changes in the power angle spectrum, with the analysis focusing on the variations in angle PS on the uniform linear array (ULA) and uniform cylindrical array, separately.

In Chen JJ et al. (2016a, 2017) and Huang J et al. (2017), variations in the statistical parameters of the array domain were investigated. Huang J et al. (2017) specifically analyzed the changes in delay spread (DS), azimuth angular spread (AAS),

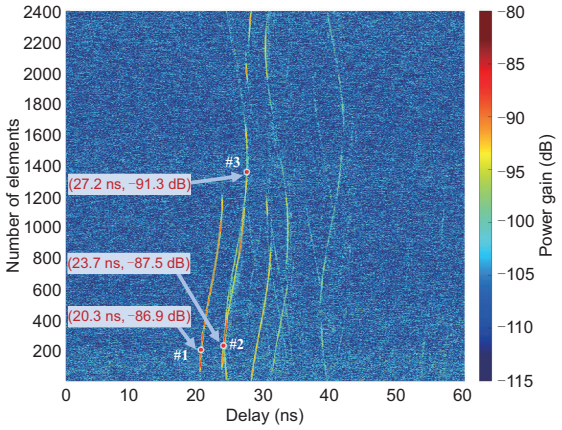

Fig. 5 Schematic representation of non-stationarity phenomena in space

and elevation angular spread (EAS) on the array domain across different frequency bands. These existing channel measurement activities focused mainly on the observation and analysis of channel characteristics, and there are fewer theoretical studies on the characterization of SnS phenomena in XL-MIMO channels.

For a more comprehensive study of XL-MIMO channels, a method that can accurately and quantitatively characterize the distribution law of SnS properties is needed. In the COST 2100 channel model, the concept of VR was introduced (Liu LF et al., 2012). In its initial definition, VR is a hypothetical region, and each VR is associated with one or more clusters. When a terminal enters a specific LoS region, the corresponding cluster is activated, and the cluster becomes invisible to the terminal when it moves out of the VR. This concept addresses the challenge of representing the active range of clusters and can serve as a quantification metric for observing the SnS of the channel.

Gao X et al. (2013) extended the concept of VR to the array domain, where only the elements within a VR on the array can observe their corresponding clusters. Therefore, the VR can be distinguished between MS-VR in the terminal domain and BS-VR in the array domain. Due to the limited physical size of the LA, the observed BS-VR may be only a partial length of the true BS-VR. To model the true BS-VR length from the observed data, the authors derived a relationship between the true BS-VR length and the observed BS-VR length. The cumulative distribution function (CDF) of the observed BS-VR length, $K_{\Delta}(y)$, can be written as a function of the probability density function (PDF) of the true BS-VR length, $f_{\alpha}(\nu)$, as

$$K_{\Delta}(y)=\begin{cases}K'_{\Delta}(y), & y\le L,\\ 1, & y>L,\end{cases} \tag{2}$$

where

$$K'_{\Delta}(y)=\int_{\Delta_0}^{y} f_{\alpha}(\nu)\mathrm{d}\nu+2y\int_{y}^{\infty}\frac{1}{L+\nu}f_{\alpha}(\nu)\mathrm{d}\nu -2\Delta_0\int_{\Delta_0}^{\infty}\frac{1}{L+\nu}f_{\alpha}(\nu)\mathrm{d}\nu, \tag{3}$$

Δ and α are the observed and true lengths of the BS-VR, respectively, L is the length of the array, and Δ_0 is the smallest observation of the BS-VR length.

At the frequency of 3.5 GHz, Wang C et al. (2017) investigated the radius of the MS-VR under different scenarios by deducing and calculating the lifecycle of clusters; the calculation results are shown in Table 3. Combined with this table, it is possible to determine the distribution characteristics of multipath clusters for XL-MIMO channels and that the number of clusters is larger in the LoS state. Combined with the statistics of the visual area radius, it can be seen that the cluster extinction changes more frequently in the NLoS state. In the three scenarios, i.e., urban macrocell (UMa), urban microcell (UMi), and indoor hotspot (InH), the number of clusters and the mean value of the visual area in the InH are both the largest, followed by UMi and UMa, successively. Yuan ZQ et al. (2023a) proposed a method based on the dominant multipath propagation mechanism to identify the SnS characteristics, which is implemented by introducing a novel matrix $\boldsymbol{S}$. It contains K nonnegative real-valued vectors, i.e.,

$$\boldsymbol{S}=[\boldsymbol{s}_1,\boldsymbol{s}_2,\cdots,\boldsymbol{s}_K], \tag{4}$$

where $\boldsymbol{s}_k=[s_{1,k},s_{2,k},\cdots,s_{M,k}]^{\mathrm{T}}$ $(k=1,2,\cdots,K)$, and $s_{m,k}$ $(m=1,2,\cdots,M)$ characterizes the SnS property of the k^{th} path on the m^{th} element. To capture the SnS contributions of multiple paths, $s_{m,k}$ is specified from the perspective of the multipath propagation mechanism as

$$s_{m,k}=\begin{cases}0, & m\notin \mathrm{VR}_k,\\ 1, & m\in \mathrm{VR}_k\ \ \&\ \ \text{blockage/reflection},\\ >0, & m\in \mathrm{VR}_k\ \ \&\ \ \text{diffraction},\end{cases} \tag{5}$$

where VR_k is defined to be the VR of the k^{th} path (i.e., elements in VR_k can view the k^{th} path, whereas elements outside VR_k cannot). Note that the $s_{m,k}$ parameter for the case of the diffraction and $m \in \mathrm{VR}_k$ can be alternatively set with the upper bound, e.g., $0 < s_{m,k} < 1$, by selecting the element with the highest power as the reference.

Table 3 Distribution of VR radius in different scenarios

Parameter		UMa		UMi		InH	
		LoS	NLoS	LoS	NLoS	LoS	NLoS
Radius of VR	μ	0.5	0.2	0.6	0.3	1.6	0.8
	σ	0.4	0.1	0.4	0.4	0.6	0.3
	Max (m)	2.6	1.1	3.1	1.7	3.6	2.2
Fitted lognormal distribution	μ	−1.6	−2.2	−1.6	−1.9	−1.3	−1.7
	σ	1.5	0.9	1.7	0.9	1.9	1.1

InH: indoor hotspot; LoS: line of sight; NLoS: non-line of sight; UMa: urban macrocell; UMi: urban microcell; VR: visible region

2. Spherical wave

XL-MIMO technology may cause the traditional far-field assumption not to hold due to the increased array aperture. In the phase aspect, the true phase of an incident electromagnetic wave on a BS antenna must be computed based on an accurate spherical wave model. In the far field, this phase is usually approximated by a first-order Taylor expansion based on a planar wavefront model, but this approximation leads to a phase discrepancy that increases when the distance decreases. The distance between the center of the BS array and the center of the user array is defined as the classical Rayleigh distance when the maximum phase difference between all BS's and user antennas reaches $\pi/8$. Therefore, if the propagation distance is smaller than the Rayleigh distance, the maximum phase difference will be greater than $\pi/8$, at which point the far-field approximation becomes inaccurate and the wave will arrive at the array as a spherical wavefront, as shown in Fig. 6. By introducing a distance parameter r, the phase of the spherical wave can be characterized as a nonlinear function of the antenna index, as

$$\phi_n = \frac{2\pi}{\lambda}\left(\sqrt{r^2 + n^2d^2 - 2ndr\sin\theta} - r\right), \quad (6)$$

where r denotes the distance from the reference array element to the user, d denotes the spacing between neighboring array elements, λ denotes the wavelength, and n denotes the antenna index.

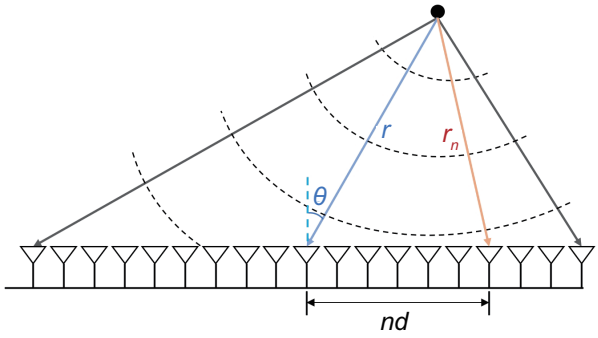

Fig. 6 Near-field spherical wave propagation

Cui and Dai (2024) demonstrated that distinguishing between near and far fields using the classical Rayleigh distance is not accurate when evaluating transmission rates. Therefore, the concept of effective Rayleigh distance is proposed to more precisely define the near-field range in terms of beamforming gains.

In Huang J et al. (2017), Li JZ et al. (2018a), Yuan ZQ et al. (2023a), and Zheng et al. (2023), the authors investigated spherical wave characteristics through channel measurement activities, and confirmed the phenomenon of spherical wavefronts by examining angular drift and delay drift from the perspective of multipath. In the near-field region, the phase of the spherical wave is accurately derived based on physical geometry and is a nonlinear function of the antenna index. Information about the incident angle and distance for each path between the BS and the user is embedded in this nonlinear phase. With the additional distance information from the spherical wavefront, near-field beamforming can focus beam energy at specific locations, achieving energy focus in the angular and distance domains. Due to this feature, near-field beamforming is also referred to as beam focusing.

3. Channel capacity

The term "favorable" was first defined as the mutual orthogonality between user channels in Ngo et al. (2013), and "favorable" propagation was further studied theoretically in Ngo et al. (2014). As the number of BS antennas increases, the channel vectors between users and BS become very long random vectors, and under "favorable" propagation conditions, these channel vectors are orthogonal to each other. Currently, the XL-MIMO system has the best capacity performance. We can also interpret favorable propagation as a sufficiently complex

scattering environment. However, in practical mobile communication scenarios, capacity performance can be affected by multiple factors.

One is the impact of the number of antennas and array structure. In the measurement study by Gao X et al. (2011), as the number of antennas gradually increases to 128, the orthogonality between users gradually increases. When the number of antennas increases to 20, close to optimal performance for two users can be achieved using a linear precoding scheme. Gao X et al. (2015) compared the total system capacity when the number of antennas at the BS is 128 and the number of users is 4 or 16, separately. When the number of users is 4, the total capacity is very close to the i.i.d. channel and can reach 75% even under adverse conditions. When the number of users is 16, the total capacity of the system reaches up to 90% of the i.i.d. channel and can reach only 50% under adverse conditions. This shows that the more the number of antennas in the BS exceeds the number of users, the better the performance of the system will be. The structure of the antenna array can also affect the capacity performance. Gao X et al. (2015) compared the channel capacity of the uniform cylindrical array and ULA with the same number of antennas. The results show that the ULA with more dispersed antennas performs better than the ULA. Under adverse conditions, using a ULA can achieve 90% of the asymptotic capacity in the i.i.d. channel, whereas using uniform cylindrical arrays can achieve only about 75%. Yang Y et al. (2022) studied the impact of mutual coupling and SnS on massive MIMO channel capacity, and proposed a spatial non-stationary channel capacity calculation method. The results obtained by the new calculation method are much larger than those of the traditional method. The verification through actual measurement and simulation illustrates the correctness of the formula.

The other impacts on the XL-MIMO channel capacity are environment and frequency. In Gao X et al. (2015), to study the multi-user performance of XL-MIMO systems under three different propagation conditions, researchers let four users be close to each other in a LoS environment, separated from each other in a LoS environment, and close to each other in an NLoS environment. The channel capacity results of the three cases show that in the NLoS environment, because the signal experiences more reflection and scattering, the orthogonality between users is stronger than that in the LoS environment, so the channel capacity is also higher. In the NLoS environment, using the uniform cylindrical array and ULA can achieve more than 90% of the asymptotic capacity of the i.i.d. channel. In the LoS environment, using the uniform cylindrical array and ULA can achieve 75% and 90% of the asymptotic value, respectively. Increasing the distance between users can also improve orthogonality. In a LoS environment, if users are kept far away from each other, performance close to asymptotic capacity can be achieved. Zhang JH et al. (2018) measured the channel capacity of XL-MIMO at 3.5 GHz and 6 GHz in UMa, UMi, and outdoor-to-indoor (O2I) scenarios. The results show that because the wavelength of 6 GHz is smaller, the signal experiences more reflections and the angles are more dispersed. Hence, the capacity performance is better than 3.5 GHz under the same receiving signal-to-noise ratio (SNR). The same SNR is set here to illustrate that under the same conditions, the 6 GHz channel can provide a higher channel capacity than the 3.5 GHz channel. However, in the actual evaluation, the propagation loss and transmission power of the communication system also need to be considered, as shown in Fig. 7. As the number of antennas increases, the capacity in the O2I scenario is relatively stable as shown in Fig. 7a, whereas in UMi and UMa scenarios, more MPCs can be captured, resulting in an increase in the channel capacity.

4. Channel hardening

As the scale of the antenna array increases, the orthogonality between users will be enhanced. In a single-input-single-output (SISO) communication system, a signal is transmitted from a single antenna and captured at the receiving antenna as a sum of constructive or destructive echoes. This results in potentially unstable SNR depending on the richness of the scattering environment. In an XL-MIMO communication system, with appropriate precoding, small-scale multipath fading is averaged over multiple transmit and receive antennas. This produces a strong reduction in received power fluctuations, so the channel gain becomes deterministic. This effect is called channel hardening. The term channel hardening was first introduced in Hochwald et al. (2004). In Ngo and Larsson (2017), a formal definition of channel hardening was given based on channel power

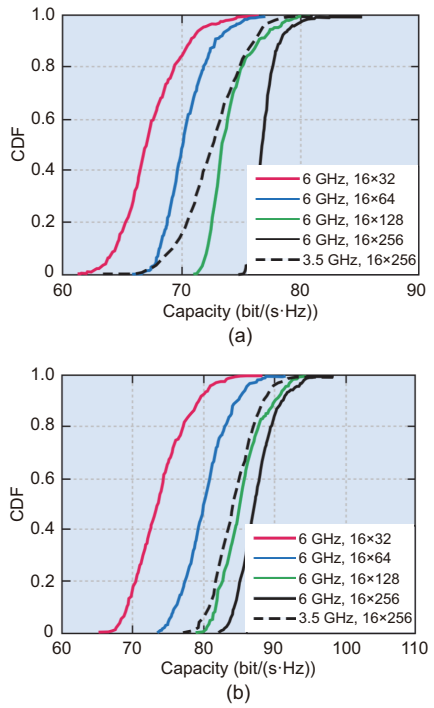

Fig. 7 Capacity CDF for XL-MIMO of 3.5 GHz and 6 GHz in different scenarios: (a) O2I; (b) UMi (CDF: cumulative distribution function; O2I: outdoor-to-indoor; UMi: urban microcell). Reprinted from Zhang JH et al. (2018), Copyright 2018, with permission from IEEE

fluctuations: propagation offers channel hardening if

$$\frac{\|\boldsymbol{g}_k\|^2}{E\left\{\|\boldsymbol{g}_k\|^2\right\}} \xrightarrow{P} 1, \text{as } M \to \infty, k = 1, 2, \ldots, K, \quad (7)$$

where $\boldsymbol{g}_k$ is the channel vector, assuming that the system has M antennas at the BS and K single-antenna users. At this time, the total capacity of the system does not depend on small-scale fading. System scheduling, power allocation, and interference management can be performed on large-scale fading time scales instead of small-scale fading time scales. As a result, the overhead of these system designs is significantly reduced. Another important advantage is that if there is channel hardening, we do not need instantaneous channel state information (CSI) at the Rx to detect the sending signal. The Rx requires only statistical information on channel gain. This reduces the resources required by channel estimates.

However, the above results are all based on optimistic assumptions about the i.i.d. channel and will be affected by the antenna and environmental factors in actual communications. Some evaluations of channel hardening were performed based on channel measurements. In Martínez et al. (2016, 2018), the effects of channel hardening in the spatial domain were studied based on two measurement campaigns at 5.8 GHz. As shown in Fig. 8a, the degree of channel hardening is better under NLoS conditions than that under LoS conditions. This is because the signal experiences more severe scattering under NLoS conditions. The measurement results under indoor LoS conditions show that when the number of antennas is the same, the larger the array aperture, the more apparent the channel hardening effect, as shown in Fig. 8b. Willhammar et al. (2018, 2020) performed a detailed analysis of the channel hardening phenomenon in indoor and outdoor scenarios in the 3.7 GHz band in the time and frequency domains. The results indicate that interactions between the array and the environment, including antenna polarization and orientation, will affect the degree of channel hardening. In addition, user movement changes the propagation environment and also affects channel hardening.

2.3.3 Summary

In this subsection, we first introduce the reasons for the SnS phenomena in XL-MIMO and demonstrate the existence of SnS through some existing XL-MIMO channel measurement campaigns. This subsection lists some results of the statistical distributions of the channel parameters, which can help in the accurate characterization of the SnS phenomena. Then we describe the reasons for the emergence of the near-field effect, list several channel measurement campaigns in which near-field spherical wave properties have been observed, and analyze the benefits and drawbacks associated with spherical waves.

Channel measurements show that the channel capacity of the XL-MIMO system is affected by the number of elements and structure of the array, the propagation environment, and the signal frequency. Favorable propagation conditions are not always achieved in actual communications. The channel conditions that are favorable for XL-MIMO are worthy of in-depth study. Similar to channel capacity, channel hardening is affected by antenna and environmental factors. To maximize empirical channel hardening, one needs to find strategies to deal with array power imbalances and design XL-MIMO systems that can best exploit the diversity of the considered environment.

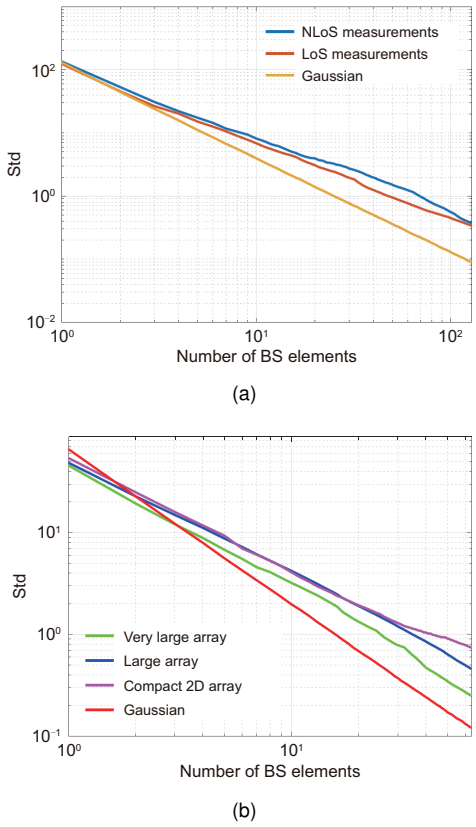

Fig. 8 Variation in mean channel vector energy of LoS/NLoS when increasing the number of BS antennas in outdoor scenarios (a) and variation in mean channel vector energy of different arrays when increasing the number of BS antennas in the indoor LoS scenario (b) (BS: base station; LoS: line of sight; NLoS: non-line of sight). Reprinted from Martínez et al. (2016), Copyright 2016, with permission from IEEE. References to color refer to the online version of this figure

3 XL-MIMO channel modeling

The assumption of planar wave and spatial stationarity is normally used in the 3GPP 38.901 channel model for 5G (3GPP, 2018). However, these assumptions are validated in XL-MIMO systems. The expanded array size results in the Fraunhofer distance being violated in a real deployment scenario. In this case, the user equipment (UE) or scatterer is most likely to be in the near field of the BS, so the more general spherical wave model should be considered for channel modeling. There are three main channel modeling methods, including statistical channel modeling, deterministic channel modeling, and hybrid channel modeling (Table 4). Next, the challenges and progress of three XL-MIMO channel modeling methods will be introduced.

3.1 Statistical channel modeling

3.1.1 Challenges

Statistical channel modeling describes the channel in a specific type of environment rather than a specific location, captures the statistical behavior of the wireless channel in different scenarios, and models the wireless channel with the help of the statistical distribution of channel parameters. The traditional statistical models assume spatial stationarity, but XL-MIMO channels exhibit SnS characteristics, and the statistical distribution of SnS characteristics of different antenna array types is different, so describing the statistical distribution is a challenge to be faced.

3.1.2 Progress

At present, there has been some research on statistical modeling methods for XL-MIMO. In López and Wang (2018), the second-order approximate channel models of spherical wavefronts (i.e., parabolic wavefronts) for XL-MIMO channels were established in spatial and temporal domains to effectively simulate the near-field effects. In Zheng et al. (2023), the general 3D non-stationary GBSM for XL-MIMO communication systems was proposed in 6G communication. As the important method for MIMO channel modeling, the COST 2100 channel model is a geometric stochastic one based on the framework of the earlier COST 259 model. The COST 259 channel model is the first one based on geometric statistics to consider multi-antenna BSs (Molisch et al., 2006). The COST 2100 model is a cluster-level GBSM for the MIMO system, which is the first to use the concept of VR to simulate SnS along the antenna array (Liu LF et al., 2012). The cluster can be viewed only through the antenna element located in the corresponding VR. However, due to the planar wave hypothesis, the modeling precision of SnS characteristics is limited in the COST 2100 model. Based on the VR concept, the GBSM with different frequency bands and scenarios was used to represent SnS and near-field effects for XL-MIMO (Li JZ et al., 2019b). However, the validity of these models may need to be further verified by measurements in real scenarios. The statistical characteristic parameters are inconsistent with the measurement, so it is difficult to extract the statistical

Table 4 XL-MIMO channel modeling methods and models

Modeling method	Model	Channel characteristic	Reference
Statistical modeling	KBSM	SnS, spherical wave	Wu et al., 2015
	WM	SnS, spherical wave	Zhai et al., 2016
	COST 2100	SnS	Gao X et al., 2013
	GBSM	Spatial consistency	Ademaj et al., 2019
	GBSM	SnS, spherical wave	Gao TY et al., 2023
	GBSM	SnS, spherical wave	Yuan ZQ et al., 2023b
	GBSM	SnS	Li JZ et al., 2019a
	GBSM	SnS, spherical wave	Jing et al., 2023
	GBSM	SnS, spherical wave	López et al., 2022
	GBSM	SnS, spherical wave	Wu et al., 2014
	COST 2100	SnS	Liu LF et al., 2012
Deterministic modeling	RT	SnS, spherical wave	Yuan ZQ et al., 2024
	RT	PL, etc.	Yao et al., 2017
Hybrid modeling	RT/GBSM	SnS	Zhang JH et al., 2024a

GBSM: geometry-based stochastic model; KBSM: Kronecker-based stochastic model; PL: path loss; RT: ray tracing; SnS: spatial non-stationarity; WM: Weichselberger model

parameters required by GBSM. It can be seen that the current XL-MIMO channel modeling based on statistics still lacks the validation and analysis of measurement data in typical communication scenarios. A pervasive channel model for diverse frequency bands and scenarios in 6G was presented in Wang CX et al. (2022). Yuan Y et al. (2022) and Wang J et al. (2023) proposed channel models for ultra-massive MIMO antenna arrays operating at the THz band. The angle-domain sparsity property of the beam-domain channel model (BDCM) can be observed, which helps reduce the complexity of the GBSM and improve mathematical tractability. The power leakage of the BDCM caused by the spherical wavefront and VR has been thoroughly analyzed. Lai et al. (2023) transformed a massive MIMO model from the antenna domain to the beam domain through specific algorithms to obtain a novel BDCM. In He YB et al. (2023), to reduce the model complexity and improve the mathematical tractability, a novel BDCM was proposed based on the transformation of the corresponding GBSM from the array domain to the beam domain for maritime communications.

Considering that the characterization and explanations of SnS have not been adequate in existing statistical channel modeling, the XL-MIMO channel modeling framework was proposed based on capturing and observing of multipath propagation mechanisms (i.e., LoS, reflection, and diffraction) (Yuan ZQ et al., 2023a), as shown in Fig. 9. Compared with the traditional statistical channel modeling, only one additional SnS parameter was added to the proposed framework, which was required for low-complexity implementation. The channeling framework is realistic, of low complexity, and accurate, which is of great value for the development of massive MIMO systems. In Yuan ZQ et al. (2023a), there were K SnS spherical propagation paths between the Tx array and Rx. The E-MIMO channel at frequency f can be modeled as a superposition of CFRs of the K paths on the array, which is the Fourier transform of CIR and expressed as

$$\boldsymbol{H}^{\mathrm{sns}}(f)=\boldsymbol{S}\odot\boldsymbol{A}(f)\cdot\boldsymbol{H}(f), \tag{8}$$

where $\boldsymbol{H}^{\mathrm{sns}}(f)$ comprises M complex values, i.e., $\boldsymbol{H}^{\mathrm{sns}}(f)\in\mathbb{C}^{M\times1}$, $f\in[f_{\mathrm{L}},f_{\mathrm{U}}]$ is the frequency within the designed range, and $\odot$ represents the elementwise product operation. $\boldsymbol{H}(f)\in\mathbb{C}^{K\times1}$ denotes CFRs at f of the K paths at the reference point.

$$\boldsymbol{H}(f)=[\alpha_1\mathrm{e}^{-\mathrm{j}2\pi f\tau_1},\alpha_2\mathrm{e}^{-\mathrm{j}2\pi f\tau_2},...,\alpha_K\mathrm{e}^{-\mathrm{j}2\pi f\tau_K}]^{\mathrm{T}}, \tag{9}$$

where α_k and τ_k $(k=1,2,...,K)$ represent the complex amplitude and propagation delay of the k^{th} path, respectively. $(\cdot)^{\mathrm{T}}$ denotes the transpose operation. $\boldsymbol{A}(f)\in\mathbb{C}^{M\times K}$ is the array manifold matrix. The manifold projected on the m^{th} antenna element by the k^{th} path, i.e., $\boldsymbol{A}$'s $(m,k)^{\mathrm{th}}$ entry $a_{m,k}$, can be represented by the transfer difference of the m^{th} element with respect to the reference point:

$$a_{m,k}(f)=\frac{\|\boldsymbol{d}_k\|}{\|\boldsymbol{d}_{m,k}\|}\mathrm{e}^{-\mathrm{j}2\pi f\frac{\|\boldsymbol{d}_{m,k}\|-\|\boldsymbol{d}_k\|}{c}}, \tag{10}$$

where c is the light speed, $\|\cdot\|$ represents the Euclidean norm of the argument, and $\boldsymbol{d}_k$ denotes the vector pointing from the reference point to the first scattering source of the k^{th} path propagation route.

To meet the 3GPP standardization requirement of the 6G channel model, a simulation framework based on 3GPP has been proposed based on the XL-MIMO channel model (Gao TY et al., 2023; Yuan ZQ et al., 2023a). In Fig. 10, the steps marked in black are the steps defined in the standard model and can be found in 3GPP TR 38.901. The steps marked in red are extended in the NF-SnS framework. Steps marked in black (steps 1–9 and 13) are the steps defined in the standard model and can be found in 3GPP TR 38.901, and steps marked in red (steps 10–12) are extended steps of the NF-SnS framework. Steps 10–12 are used to obtain $\boldsymbol{S}$, calculate $\boldsymbol{A}$, and generate channel coefficients with near field (NF) and SnS characteristics. The BS is configured with a ULA of K array elements and the user terminal (UT) is configured with a single antenna. Configurations of BS and UT can be easily extended to a UPA, uniform circular array, or other configurations.

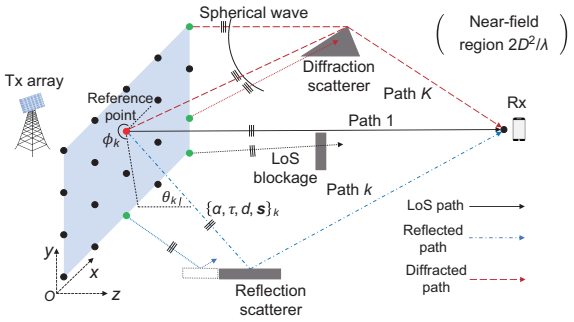

Fig. 9 Spherical propagation with spatial non-stationarity (SnS) characteristics in the near-field region. Three cases that contribute to SnS propagation, line of sight (LoS) blockage, incomplete reflection, and diffraction, were illustrated in Yuan ZQ et al. (2023a). Reprinted from Yuan ZQ et al. (2023a), Copyright 2023, with permission from IEEE

3.1.3 Summary

The current GBSM model makes it difficult to characterize the near-field and SnS characteristics of XL-MIMO. Although the GBSM model has evolved in the existing research, most statistical models differ greatly from the 3GPP standard model, and it is difficult to develop the near-field simulation process under the existing 3GPP simulation framework. To solve the problem, a feasible 3GPP simulation framework is proposed, but a lot of measurement work needs to be carried out in the real communication environment to extract the model parameters. The complexity of the statistical channel model is low, but it needs a highly reliable channel measurement platform that can measure XL-MIMO channel characteristics.

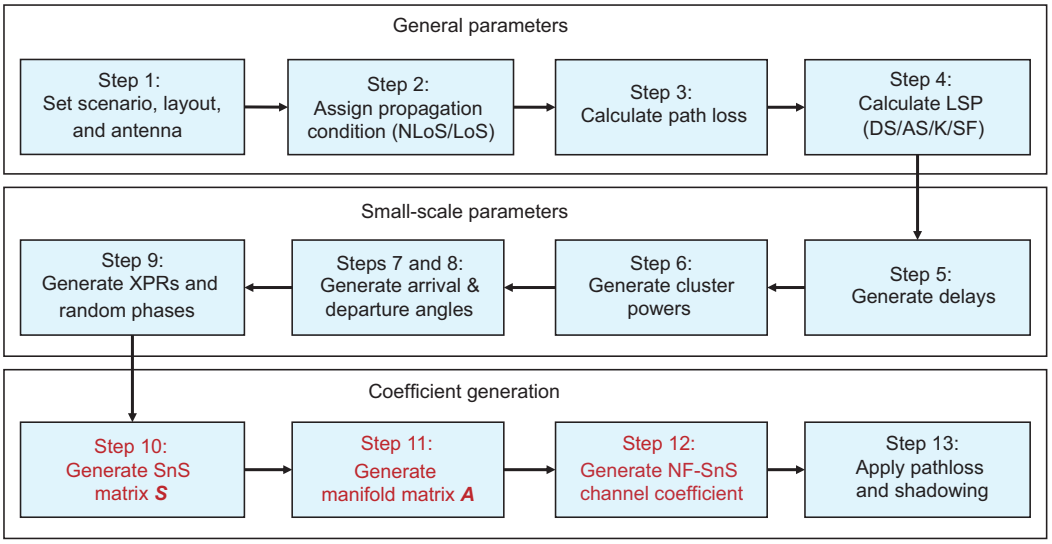

Fig. 10 Flowchart of the NF-SnS framework (NF: near field; SnS: spatial non-stationarity). Reprinted from Gao TY et al. (2023), Copyright 2023, with permission from IEEE. References to color refer to the online version of this figure

3.2 Deterministic channel modeling

3.2.1 Challenges

Compared with statistical channel modeling, deterministic channel modeling can accurately capture electromagnetic wave propagation characteristics, which depends on the propagation environment of the study scenario, the dielectric parameters of the material, and the detailed geometric information of the spatial position of the transceiver antenna. In addition, there are many challenges for deterministic channel modeling. First, it is difficult to obtain the material electromagnetic medium parameters required for deterministic modeling. Second, the accuracy of channel data obtained by simulation depends on the high-precision communication scenario model. Finally, as the number of XL-MIMO array elements increases, the complexity increases exponentially.

3.2.2 Progress

There are several different types of deterministic modeling methods. The METIS project (Yuan ZQ et al., 2024) proposed a massive MIMO channel model based on ray tracing (RT) technology, which can characterize SnS properties. No matter the size of massive MIMO arrays, the RT method can accurately capture channel characteristics, which makes it a promising channel modeling method for massive MIMO systems (Wang CW et al., 2016; Tamaddondar and Noori, 2019). However, only a few works have implemented RT to characterize channels with XL-MIMO configurations. The reason is that the arrays on the Tx and Rx sides are usually obtained by strong simulation of each Tx and Rx antenna pair in RT. The computational complexity is particularly challenging for massive MIMO systems because it increases linearly with the number of array elements. At present, the map-based model is proposed to implement the RT method, which can effectively reduce the computational complexity by simplifying the geometry and electromagnetic description of the environment and restricting the sequence of interactions between the rays and objects (Yao et al., 2017). The model may have poor accuracy in predicting the channel at specific locations, but it is fully capable of simulating the non-stationarity and transition of XL-MIMO. However, the high computational complexity and lack of detailed digital maps and material databases make the deterministic modeling method less applicable in some scenarios with complex environments. It can be seen that the SnS characteristics and spherical waves of XL-MIMO can be well characterized by RT simulation. The trajectory of MPCs across the array elements is almost the same between the RT results and the measurement results. Specifically, three strong MPCs are marked in numbers. Good agreement is achieved among the measurement and RT simulated paths in terms of power, angle, and delay (Zhang JH et al., 2024a). Note that the standard geometry based stochastic channel modeling approaches would fail to model such near-field and SnS effects. It can be seen that deterministic modeling has advantages in capturing the SnS properties of XL-MIMO. Yuan ZQ et al. (2024) aimed at accurate and efficient RT simulations for XL-MIMO systems, with a proposed coarse-refinement strategy capable of capturing NF and SnS, as shown in Fig. 11. The channel is simulated using RT on a few sparsely located array elements and then interpolated onto other elements using spherical/astigmatic-wave approximation and the uniform theory of diffraction, thus significantly reducing simulation complexity while maintaining accuracy. The coarse-refinement method achieves around 99.5% modeling accuracy and 94.3% acceleration efficiency compared to the brute-force method for all three measurement scenarios (one LoS and two obstructed-line of sights (OLoSs)).

3.2.3 Summary

For XL-MIMO channel characterization, the deterministic modeling method has high precision. However, due to the large number of antenna elements, simulations require geometric tracking of interaction points for each pair of antenna elements, resulting in high complexity. In the literature, some solutions to reduce complexity have been proposed, but there is no optimal criterion for judgment. In addition, the lack of knowledge of EM properties and the computational complexity hinder the use of the XL-MIMO deterministic modeling method.

3.3 Hybrid channel modeling

3.3.1 Challenges

The deterministic channel modeling method sacrifices time and computational resources to

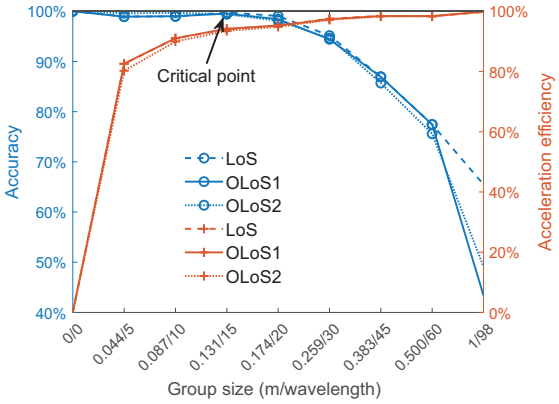

Fig. 11 Analysis of the simulation complexity (corresponding to acceleration efficiency) and accuracy of the coarse-refinement method of deterministic channel modeling. For the brute-force method, we denote the group size as "0/0" since RT simulations are performed for each element (i.e., one element in a group). Reprinted from Yuan ZQ et al. (2024), Copyright 2024, with permission from IEEE. References to color refer to the online version of this figure

improve modeling accuracy, while the statistical channel modeling method reduces the computational complexity of the model at the cost of accuracy. Therefore, there is a tendency to study XL-MIMO hybrid channel modeling methods by combining the advantages of two or more channel modeling methods. However, some challenges exist, including the basic modeling principles and methods, how these channel modeling methods are specifically combined, and the balance between complexity and precision. Therefore, to capture the new characteristics of the XL-MIMO channel, low complexity and high accuracy are important challenges for hybrid channel modeling.

3.3.2 Progress

For hybrid channel modeling, there is some work involved in XL-MIMO modeling. By applying the finite-difference time-domain (FDTD) method to only a small part of the RT-FDTD hybrid technology, the accuracy of the entire modeling environment can be maintained while the calculation time is improved, and the remaining work is completed by RT simulation (Reynaud et al., 2006). This hybrid method is suitable for mmWave and THz channels. In Chen Y et al. (2021), a semi-deterministic channel model was established for a 140 GHz indoor channel using a hybrid modeling method, in which the von Mises distribution was used to generate the arrival angles of inter- and intra-cluster multipaths. It can be seen that the hybrid modeling method combining statistical and deterministic modeling is expected to reduce the complexity of the model because only the dominant path has RT characteristics. However, at present, the hybrid channel modeling method has not been proved to be good for XL-MIMO channel modeling, which belongs to one of the future research directions.

Fig. 12 shows a hybrid modeling method based on measurement calibration for XL-MIMO. Based on the measurements, the material's EM properties are adjusted in RT simulation to reach the best agreement in terms of power and delay for the dominant propagation paths (Zhang JH et al., 2024a). In the beginning, the RT simulation outputs the results corresponding to the initial EM parameters, which are compared with the measurement data. If the results of the power and delay parameters for the dominant paths match (to minimize the root mean square error), the simulation results are outputted. If the results do not match, the relative permittivity and conductivity of the materials are updated and the simulation results are outputted again. This operation is repeated until the best agreement between the simulation and measurement results is achieved. The maximum differences of AoA, azimuth of departure (AoD), delay, and power gain of the dominant paths are $-1.8°$, $-1.5°$, 0.7 ns, and -0.7 dB, respectively, while the minimum differences come from the first path, up to $-1.7°$, $0.3°$, -0.1 ns, and 0 dB, respectively (Zhang JH et al., 2024a). In conclusion, the hybrid modeling method can achieve a better trade-off between precision and complexity.

3.3.3 Summary

At present, there is no unified definition of hybrid channel modeling methods for XL-MIMO. There is a tendency to study hybrid modeling methods by combining the advantages of two or more channel modeling methods, but they are rarely used for XL-MIMO channel modeling. Although some work has been conducted to realize channel modeling of XL-MIMO by modifying EM parameters through actual measurement and combining deterministic modeling ideas, the accuracy and complexity of the hybrid method that can capture new features of XL-MIMO channels need to be considered.

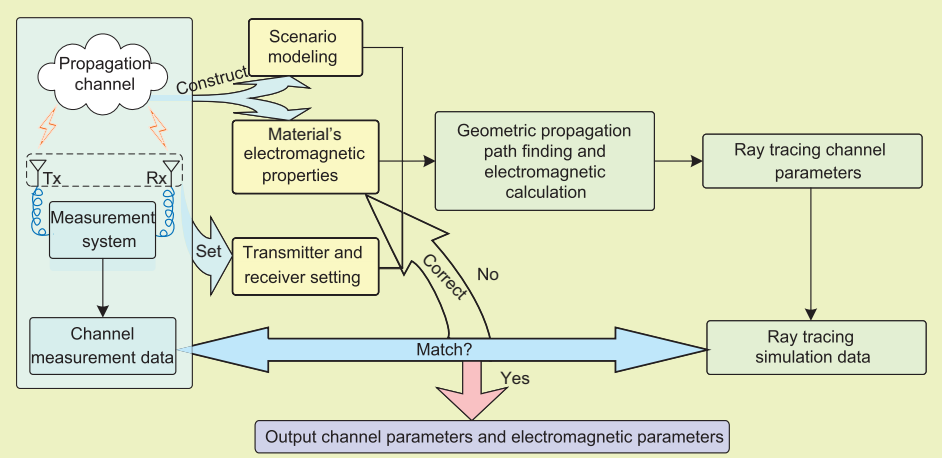

Fig. 12 Flowchart of measurement-calibrated hybrid channel modeling. Reprinted from Zhang JH et al. (2024a), Copyright 2024, with permission from IEEE

4 Open issues in XL-MIMO channel measurement, characterization, and modeling

Though there has been a certain amount of research on XL-MIMO channel measurement, characterization, and modeling, some issues have not been adequately resolved. In this section we discuss some important open issues in these fields to provide a reference for future XL-MIMO channel research.

4.1 Cost- and time-efficient channel sounder

A channel sounder is a prerequisite for recording raw channel data, which is crucial in channel characterization and modeling. Usually, the channel sounder should have high resolution in the time, spatial, or frequency domain to accurately sample raw channel data (Ferreira et al., 2015). Considering that the hybrid beamforming (HBF) technique could generate a narrow beam in XL-MIMO communication systems, an XL-MIMO channel sounder should have a spatial resolution as the beamwidth to at least satisfy the need for system performance evaluation. However, as the number of antenna elements at the BS increases to hundreds, even thousands, it is highly costly or time-consuming. For the channel sounder built with RAAs, the amplifier, switch unit, and antenna array are costly, especially in mmWave and THz bands. A MIMO channel sounder with over 100 antenna Tx elements may cost hundreds of thousands or millions of dollars. For the channel sounder built with VAAs, an antenna element or antenna sub-array is moved in the spatial domain to produce a large-scale and VAA (Zhang JH et al., 2018). In each measurement position, hundreds of movements are needed to capture XL-MIMO channel characteristics, which may take hours. This brings a serious challenge to the stationarity assumption during channel measurements, and a time-variant channel cannot be measured by using this kind of method. Thus, a new kind of channel sounder that can be built in a cost-efficient way and be operated in a time-effective way should be proposed in the future.

4.2 Non-stationarity in spatial, frequency, and time domains

Wide sense stationary uncorrelated scattering (WSSUS) is a fundamental assumption in wireless channel modeling, especially in MIMO channel modeling (Molisch, 2005). Channel stationarity means that the statistical properties of the channel remain constant. With this assumption, statistical methods can be used to describe channel behavior. However, this assumption is more likely to be violated in practical XL-MIMO channels. In the spatial domain, channels viewed from different antenna elements may show different properties, which was discussed in the previous sections. Furthermore, as the position of BS or UE changes, scatterers and obstacles in the propagation environment between the BS and the UE would correspondingly vary and induce changes in statistical properties. In the frequency domain, statistical properties show frequency dependency as presented in 3GPP TR 38.901. For example, the

mean value of DS linearly decreases with the increase of the frequency. Furthermore, as the frequency increases, the power gain is more likely to concentrate in a few multipaths, which makes the channel sparse (Liu XM et al., 2023). Correspondingly, the number of clusters may decrease, and the cluster structure may change. Currently, some frequency bands have attracted wide attention and research, such as mid-band (Miao et al., 2023; Zhang JH et al., 2024b). Specifically, with deploying XL-MIMO in new spectrums (7–24 GHz, THz bands), a large frequency span will result in an apparent variance of statistical properties (Zhang JH et al., 2024b). In the time domain, time-varying channels feature significant Doppler spread in addition to DS. Thus, when scatterers in the propagation environment or UEs are mobile, statistical properties also show non-stationarity in the time domain. In general, non-stationarity in the spatial, frequency, and time domains in XL-MIMO channels should be further investigated and characterized.

4.3 New channel characteristics arising from combination with other technologies

To obtain better capabilities, XL-MIMO is expected to combine other enabling technologies, e.g., RIS and ISAC. Subsequently, new channel characteristics arise and should be considered in channel modeling. For example, RIS can be densely deployed to enhance the coverage capability in key regions at a low cost (Sang et al., 2024). If the RIS is close to the UE, the RIS–UE link may be in the near-field range while the BS–RIS link may be in the far-field range, which induces a hybrid-field characteristic. Also, RIS radiation pattern characteristics should be described in channel models. Furthermore, ISAC is one of six new usage scenarios defined in ITU-R M.2160 (ITU-R, 2023); it integrates perception and communication systems to improve the efficiency of hardware, spectrum, time, and energy. Also, the high-resolution capability of XL-MIMO systems in the spatial domain can significantly intensify the sensing accuracy. However, this combination would bring new channel characteristics, e.g., the radar cross-section (RCS) and sharing clusters between the sensing channel and the communication channel (Liu YM et al., 2024). RCS is the key parameter to describe the target in the sensing channel. Because it is related to the incidence angle of sensing signals, the spherical-wave effect in the near-field region may make the RCS vary across the antenna array. Moreover, although there are sharing clusters that can create simplification when simultaneously modeling sensing and communication channels, other non-shared clusters may have different VR and bring essential needs for modeling the sensing channel and the communication channel separately.

4.4 Antenna-independent channel characterization and modeling

A radio channel model is used to describe the wave propagation between Tx and Rx, in which the antenna pattern and propagation phenomena (e.g., specular reflections and diffuse scattering) are characterized. To make the radio channel model suitable for any type of antenna, antenna-independent modeling should be guaranteed, which allows antenna de-embedding and embedding (Landmann, 2008). However, XL-MIMO brings challenges to getting this guarantee. First, the 3D radiation patterns of practical antenna arrays are required when using high-resolution channel parameter extraction algorithms (Fleury et al., 2002). As the number of antenna elements increases to hundreds, it is costly and time-consuming to measure the 3D radiation patterns in an anechoic chamber. In addition, there are very few anechoic chambers that can measure 3D radiation patterns in THz bands. Second, visibility regions of scatterers at the BS depend on the shape of antenna arrays. For example, a UPA would see different visibility regions compared to an (omnidirectional array) ODA in the same propagation environment. Correspondingly, channel measurements with different kinds of antenna arrays may obtain different channel statistical properties. Third, current propagation channel models normally assume that the antennas used at the BS and UE are isotropic point sources that radiate power in all directions. Practical antenna effects on channel properties are not described. Though the radio pattern of antenna arrays is embedded in the radio channel model, it is necessary to further decouple channel statistical properties and antennas.

4.5 Intelligent channel modeling

Except in combining XL-MIMO with new enabling technologies, e.g., RIS and ISAC, XL-MIMO

would be deployed in various scenarios, e.g., the Industrial Internet of Things (IIoT) and space–air–ground-integrated network (SAGIN). Predictably, there would be a consistent growth in the number of antenna elements, frequency, and scenarios (Zhang JH et al., 2023). Motivated by this growth, XL-MIMO channel modeling would experience unprecedented growth in complexity. Channel modeling can be divided into deterministic and stochastic approaches. Though multipaths are generated efficiently based on channel statistical properties, the simulation complexity would have an exponential growth as the number of antenna elements increases. Also, new channel characteristics mean that XL-MIMO channel modeling faces unprecedented challenges, which may not be dealt with by current channel modeling methods. In addition, AI and data mining technologies have rapidly evolved and can be a powerful tool inducing complexity in channel modeling. Zhang JH (2016) proposed a cluster-nuclei-based channel model that uses data mining technologies to characterize core clusters. This model has low complexity and a limited number of cluster-nuclei, and the cluster-nuclei are physically mapped to real propagation objects. However, this physical mapping is complex and not easy to obtain. Generally, intelligent channel modeling is a promising research direction, but it is in its infancy, and more powerful neural networks or learning algorithms should be proposed and applied.

5 Conclusions

XL-MIMO channel research is crucial for the development, standardization, and application of XL-MIMO technologies. In this paper, the challenges and recent progress of XL-MIMO channel measurement, characterization, and modeling are discussed in detail. In terms of XL-MIMO channel measurement, compared with using an RAA, using a VAA is simple to operate, low in cost, and more commonly used. However, this method takes a long time to acquire a round of data, so it is difficult to cope with the highly dynamic application scenarios of 6G.

As for XL-MIMO channel characterization, SnS, spherical wave, and channel capacity in XL-MIMO channels have been investigated based on channel measurements. Some characterization methods have also been proposed to model these characteristics. However, more realistic and low-complexity methods are needed to accurately describe them.

Regarding XL-MIMO channel modeling, faced with the need for 3GPP standardization of channel models, statistical channel modeling methods lack statistical analysis based on measurement data, whereas deterministic channel modeling and hybrid channel modeling methods need to fully consider the balance between complexity and precision.

Finally, some open issues in XL-MIMO channel measurement, characterization, and modeling are presented, including cost-effective and time-efficient channel sounders, non-stationarity in spatial, frequency, and time domains, new channel characteristics arising from a combination with other technologies, and intelligent channel modeling. These can give some insights into future XL-MIMO channel research.

Contributors

Jianhua ZHANG proposed the idea. Pan TANG, Haiyang MIAO, Qi WEI, and Weirang ZUO drafted the paper. Lei TIAN, Tao JIANG, and Guangyi LIU revised and finalized the paper.

Conflict of interest

Jianhua ZHANG is an executive associate editor-in-chief of *Frontiers of Information Technology & Electronic Engineering*, and Guangyi LIU is a corresponding expert of *Frontiers of Information Technology & Electronic Engineering*; they were not involved with the peer review process of this paper. All the other authors declare that they have no conflict of interest.

References

3GPP, 2018. Study on Channel Model for Frequencies from 0.5 to 100 GHz. 3GPP TR 38.901.

Ademaj F, Schwarz S, Berisha T, et al., 2019. A spatial consistency model for geometry-based stochastic channels. *IEEE Access*, 7:183414-183427. https://doi.org/10.1109/ACCESS.2019.2958154

Chen JJ, Yin XF, Wang S, 2016a. Measurement-based massive MIMO channel modeling in 13–17 GHz for indoor hall scenarios. IEEE Int Conf on Communications, p.1-5. https://doi.org/10.1109/ICC.2016.7511276

Chen JJ, Wang S, Yin XF, 2016b. A spherical-wavefront-based scatterer localization algorithm using large-scale antenna arrays. *IEEE Commun Lett*, 20(9):1796-1799. https://doi.org/10.1109/LCOMM.2016.2585478

Chen JJ, Yin XF, Cai XS, et al., 2017. Measurement-based massive MIMO channel modeling for outdoor LoS and NLoS environments. *IEEE Access*, 5:2126-2140. https://doi.org/10.1109/ACCESS.2017.2652983

Chen Y, Li YB, Han C, et al., 2021. Channel measurement and ray-tracing-statistical hybrid modeling for low-terahertz indoor communications. *IEEE Trans Wirel Commun*, 20(12):8163-8176. https://doi.org/10.1109/TWC.2021.3090781

Cui MY, Dai LL, 2024. Near-field wideband beamforming for extremely large antenna arrays. *IEEE Trans Wirel Commun*, 23(10):13110-13124. https://doi.org/10.1109/TWC.2024.3398770

Cui MY, Wu ZD, Lu Y, et al., 2023. Near-field MIMO communications for 6G: fundamentals, challenges, potentials, and future directions. *IEEE Commun Mag*, 61(1):40-46. https://doi.org/10.1109/MCOM.004.2200136

Dala Pegorara Souto V, Dester PS, Soares Pereira Facina M, et al., 2023. Emerging MIMO technologies for 6G networks. *Sensors*, 23(4):1921. https://doi.org/10.3390/s23041921

de Figueiredo FAP, 2022. An overview of massive MIMO for 5G and 6G. *IEEE Lat Am Trans*, 20(6):931-940. https://doi.org/10.1109/TLA.2022.9757375

Fayad Y, Wang CY, Cao QS, et al., 2015. A developed ESPRIT algorithm for DOA estimation. *Frequenz*, 69(5-6):263-269. https://doi.org/10.1515/freq-2014-0112

Ferreira D, Caldeirinha RFS, Leonor N, 2015. Real-time high-resolution radio frequency channel sounder based on the sliding correlation principle. *IET Microw Antenn Propag*, 9(8):837-846. https://doi.org/10.1049/iet-map.2014.0165

Fleury BH, Jourdan P, Stucki A, 2002. High-resolution channel parameter estimation for MIMO applications using the SAGE algorithm. Int Zurich Seminar on Broadband Communications Access-Transmission-Networking, p.30. https://doi.org/10.1109/IZSBC.2002.991773

Gaillot DP, Tanghe E, Stefanut P, et al., 2011. Accuracy of specular path estimates with ESPRIT and RiMAX in the presence of measurement-based diffuse multipath components. Proc 5th European Conf on Antennas and Propagation, p.3619-3622.

Gao TY, Tang P, Tian L, et al., 2023. A 3GPP-like channel simulation framework considering near-field spatial non-stationary characteristics of massive MIMO. IEEE Globecom Workshops, p.1493-1498. https://doi.org/10.1109/GCWkshps58843.2023.10464808

Gao X, Edfors O, Rusek F, et al., 2011. Linear pre-coding performance in measured very-large MIMO channels. IEEE Vehicular Technology Conf, p.1-5. https://doi.org/10.1109/VETECF.2011.6093291

Gao X, Tufvesson F, Edfors O, et al., 2012. Measured propagation characteristics for very-large MIMO at 2.6 GHz. 46th Asilomar Conf on Signals, Systems and Computers, p.295-299. https://doi.org/10.1109/ACSSC.2012.6489010

Gao X, Tufvesson F, Edfors O, 2013. Massive MIMO channels—measurements and models. Asilomar Conf on Signals, Systems and Computers, p.280-284. https://doi.org/10.1109/ACSSC.2013.6810277

Gao X, Edfors O, Rusek F, et al., 2015. Massive MIMO performance evaluation based on measured propagation data. *IEEE Trans Wirel Commun*, 14(7):3899-3911. https://doi.org/10.1109/TWC.2015.2414413

Gong TR, Gavriilidis P, Ji R, et al., 2024. Holographic MIMO communications: theoretical foundations, enabling technologies, and future directions. *IEEE Commun Surv Tutor*, 26(1):196-257. https://doi.org/10.1109/COMST.2023.3309529

He J, Swamy MNS, Ahmad MO, 2012. Efficient application of MUSIC algorithm under the coexistence of far-field and near-field sources. *IEEE Trans Signal Process*, 60(4):2066-2070. https://doi.org/10.1109/TSP.2011.2180902

He YB, Wang CX, Chang HT, et al., 2023. A novel 3-D beam domain channel model for maritime massive MIMO communication systems using uniform circular arrays. *IEEE Trans Commun*, 71(4):2487-2502. https://doi.org/10.1109/TCOMM.2023.3245662

Hochwald BM, Marzetta TL, Tarokh V, 2004. Multiple-antenna channel hardening and its implications for rate feedback and scheduling. *IEEE Trans Inform Theory*, 50(9):1893-1909. https://doi.org/10.1109/TIT.2004.833345

Hong JX, Rodríguez-Piñeiro J, Yin XF, et al., 2023. Joint channel parameter estimation and scatterers localization. *IEEE Trans Wirel Commun*, 22(5):3324-3340. https://doi.org/10.1109/TWC.2022.3217560

Huang J, Wang CX, Feng R, et al., 2017. Multi-frequency mmWave massive MIMO channel measurements and characterization for 5G wireless communication systems. *IEEE J Sel Areas Commun*, 35(7):1591-1605. https://doi.org/10.1109/JSAC.2017.2699381

Huang YD, Barkat M, 1991. Near-field multiple source localization by passive sensor array. *IEEE Trans Antenn Propag*, 39(7):968-975. https://doi.org/10.1109/8.86917

Huo YM, Lin XQ, Di BY, et al., 2023. Technology trends for massive MIMO towards 6G. *Sensors*, 23(13):6062. https://doi.org/10.3390/s23136062

ITU-R, 2023. Framework and Overall Objectives of the Future Development of IMT for 2030 and Beyond. https://www.itu.int/dms_pubrec/itu-r/rec/m/R-REC-M.2160-0-202311-I!!PDF-E.pdf [Accessed on Oct. 10, 2024].

Jing GZ, Hong JX, Yin XF, et al., 2023. Measurement-based 3-D channel modeling with cluster-of-scatterers estimated under spherical-wave assumption. *IEEE Trans Wirel Commun*, 22(9):5828-5843. https://doi.org/10.1109/TWC.2023.3237564

Ju SH, Rappaport TS, 2021. Sub-terahertz spatial statistical MIMO channel model for urban microcells at 142 GHz. IEEE Global Communications Conf, p.1-6. https://doi.org/10.1109/GLOBECOM46510.2021.9685929

Lai F, Wang CX, Huang J, et al., 2023. A novel beam domain channel model for B5G massive MIMO wireless communication systems. *IEEE Trans Veh Technol*, 72(4):4143-4156. https://doi.org/10.1109/TVT.2022.3222771

Landmann M, 2008. Limitations of Experimental Channel Characterisation. PhD Thesis, Technische Universität Ilmenau, Germany.

Li JX, Zhao YP, 2014. Channel characterization and modeling for large-scale antenna systems. 14th Int Symp on Communications and Information Technologies, p.559-563. https://doi.org/10.1109/ISCIT.2014.7011977

Li JZ, Ai B, He RS, et al., 2017. Characterization of indoor massive MIMO channel at 11 GHz. 32nd General Assembly and Scientific Symp of the International Union of Radio Science, p.1-4. https://doi.org/10.23919/URSIGASS.2017.8105378

Li JZ, Ai B, He RS, et al., 2018a. The 3D spatial non-stationarity and spherical wavefront in massive MIMO channel measurement. 10th Int Conf on Wireless Communications and Signal Processing, p.1-6. https://doi.org/10.1109/WCSP.2018.8555869

Li JZ, Ai B, He RS, et al., 2018b. Directional analysis of massive MIMO channels at 11 GHz in theater environment. 88th Vehicular Technology Conf, p.1-5. https://doi.org/10.1109/VTCFall.2018.8690661

Li JZ, Ai B, He RS, et al., 2019a. A cluster-based channel model for massive MIMO communications in indoor hotspot scenarios. *IEEE Trans Wirel Commun*, 18(8):3856-3870. https://doi.org/10.1109/TWC.2019.2919026

Li JZ, Ai B, He RS, et al., 2019b. On 3D cluster-based channel modeling for large-scale array communications. *IEEE Trans Wirel Commun*, 18(10):4902-4914. https://doi.org/10.1109/TWC.2019.2930694

Li MT, Yuan ZQ, Lyu YJ, et al., 2023. Gigantic MIMO channel characterization: challenges and enabling solutions. *IEEE Commun Mag*, 61(10):140-146. https://doi.org/10.1109/MCOM.001.2200969

Liu L, Tao C, Matolak DW, et al., 2015. Stationarity investigation of a LOS massive MIMO channel in stadium scenarios. 82nd Vehicular Technology Conf, p.1-5. https://doi.org/10.1109/VTCFall.2015.7391154

Liu LF, Oestges C, Poutanen J, et al., 2012. The COST 2100 MIMO channel model. *IEEE Wirel Commun*, 19(6):92-99. https://doi.org/10.1109/MWC.2012.6393523

Liu MY, Zhang Y, Jin YS, et al., 2024. Towards near-field communications for field communications for 6G: challenges and opportunities. *ZTE Commun*, 22(1):3-15. https://doi.org/10.12142/ZTECOM.202401002

Liu XM, Zhang JH, Tang P, et al., 2023. Channel sparsity variation and model-based analysis on 6, 26, and 132 GHz measurements. https://doi.org/10.48550/arXiv.2302.08772

Liu YM, Zhang JH, Zhang YX, et al., 2024. A shared cluster-based stochastic channel model for integrated sensing and communication systems. *IEEE Trans Veh Technol*, 73(5):6032-6044. https://doi.org/10.1109/TVT.2023.3337648

Liu YW, Xu JQ, Wang ZL, et al., 2023. Simultaneously transmitting and reflecting (STAR) RISs for 6G: fundamentals, recent advances, and future directions. *Front Inform Technol Electron Eng*, 24(12):1689-1707. https://doi.org/10.1631/FITEE.2300490

López CF, Wang CX, 2018. Novel 3-D non-stationary wideband models for massive MIMO channels. *IEEE Trans Wirel Commun*, 17(5):2893-2905. https://doi.org/10.1109/TWC.2018.2804385

López CF, Wang CX, Zheng Y, 2022. A 3D non-stationary wideband massive MIMO channel model based on ray-level evolution. *IEEE Trans Commun*, 70(1):621-634. https://doi.org/10.1109/TCOMM.2021.3120757

Lyu YJ, Mbugua AW, Olesen K, et al., 2021. Design and validation of the phase-compensated long-range sub-THz VNA-based channel sounder. *IEEE Antenn Wirel Propag Lett*, 20(12):2461-2465. https://doi.org/10.1109/LAWP.2021.3114626

Martínez AO, de Carvalho E, Nielsen JØ, 2016. Massive MIMO properties based on measured channels: channel hardening, user decorrelation and channel sparsity. 50th Asilomar Conf on Signals, Systems and Computers, p.1804-1808. https://doi.org/10.1109/ACSSC.2016.7869694

Martínez AO, Nielsen JØ, de Carvalho E, et al., 2018. An experimental study of massive MIMO properties in 5G scenarios. *IEEE Trans Antenn Propag*, 66(12):7206-7215. https://doi.org/10.1109/TAP.2018.2871881

Mbugua AW, Chen Y, Ji YL, et al., 2024. Experimental analysis of the multipath lifetime in indoor millimeter-wave channels. *IEEE Antenn Wirel Propag Lett*, 23(1):129-133. https://doi.org/10.1109/LAWP.2023.3319349

Miao HY, Zhang JH, Tang P, et al., 2023. Sub-6 GHz to mmWave for 5G-advanced and beyond: channel measurements, characteristics and impact on system performance. *IEEE J Sel Areas Commun*, 41(6):1945-1960. https://doi.org/10.1109/JSAC.2023.3274175

Miao HY, Tang P, Zhang JH, et al., 2024. Measurement-based massive MIMO channel characterization in 6 GHz band for 6G. IEEE Wireless Communications and Networking Conf, p.1-6.

Molisch AF, 2005. Ultrawideband propagation channels-theory, measurement, and modeling. *IEEE Trans Veh Technol*, 54(5):1528-1545. https://doi.org/10.1109/TVT.2005.856194

Molisch AF, 2011. Wireless Communications (2nd Ed.). John Wiley & Sons, Chichester, UK.

Molisch AF, Asplund H, Heddergott R, et al., 2006. The COST259 directional channel model—part I: overview and methodology. *IEEE Trans Wirel Commun*, 5(12):3421-3433. https://doi.org/10.1109/TWC.2006.256966

Mudonhi A, D'Errico R, Oestges C, 2020. Indoor mmWave channel characterization with large virtual antenna arrays. 14th European Conf on Antennas and Propagation, p.1-5. https://doi.org/10.23919/EuCAP48036.2020.9135628

Ngo HQ, Larsson EG, 2017. No downlink pilots are needed in TDD massive MIMO. *IEEE Trans Wirel Commun*, 16(5):2921-2935. https://doi.org/10.1109/TWC.2017.2672540

Ngo HQ, Larsson EG, Marzetta TL, 2013. Energy and spectral efficiency of very large multiuser MIMO systems. *IEEE Trans Commun*, 61(4):1436-1449. https://doi.org/10.1109/TCOMM.2013.020413.110848

Ngo HQ, Larsson EG, Marzetta TL, 2014. Aspects of favorable propagation in massive MIMO. 22nd European Signal Processing Conf, p.76-80.

Payami S, Tufvesson F, 2012. Channel measurements and analysis for very large array systems at 2.6 GHz. 6th European Conf on Antennas and Propagation, p.433-437. https://doi.org/10.1109/EuCAP.2012.6206345

Regier MD, Moodie EEM, 2016. The orthogonally partitioned EM algorithm: extending the EM algorithm for

algorithmic stability and bias correction due to imperfect data. *Int J Biostat*, 12(1):65-77. https://doi.org/10.1515/ijb-2015-0016

Reynaud S, Cocheril Y, Vauzelle R, et al., 2006. Hybrid FDTD/UTD indoor channel modeling. Application to WiFi transmission systems. IEEE Vehicular Technology Conf, p.1-5. https://doi.org/10.1109/VTCF.2006.42

Rusek F, Persson D, Lau BK, et al., 2013. Scaling up MIMO: opportunities and challenges with very large arrays. *IEEE Signal Process Mag*, 30(1):40-60. https://doi.org/10.1109/MSP.2011.2178495

Saad W, Bennis M, Chen MZ, 2020. A vision of 6G wireless systems: applications, trends, technologies, and open research problems. *IEEE Netw*, 34(3):134-142. https://doi.org/10.1109/MNET.001.1900287

Saleh AAM, Valenzuela R, 1987. A statistical model for indoor multipath propagation. *IEEE J Sel Areas Commun*, 5(2):128-137. https://doi.org/10.1109/JSAC.1987.1146527

Sang J, Yuan YF, Tang WK, et al., 2024. Coverage enhancement by deploying RIS in 5G commercial mobile networks: field trials. *IEEE Wirel Commun*, 31(1):172-180. https://doi.org/10.1109/MWC.011.2200356

Schmidt R, 1986. Multiple emitter location and signal parameter estimation. *IEEE Trans Antenn Propag*, 34(3):276-280. https://doi.org/10.1109/TAP.1986.1143830

Tamaddondar MM, Noori N, 2019. 3D massive MIMO channel modeling with cluster based ray tracing method. 27th Iranian Conf on Electrical Engineering, p.1249-1253. https://doi.org/10.1109/IranianCEE.2019.8786414

Wang C, Zhang JH, Tian L, et al., 2017. The spatial evolution of clusters in massive MIMO mobile measurement at 3.5 GHz. 85th Vehicular Technology Conf, p.1-6. https://doi.org/10.1109/VTCSpring.2017.8108242

Wang CW, Papadopoulos H, Kitao K, et al., 2016. Ray-tracing based performance evaluation of 5G mmWave massive MIMO in hotspots. Int Symp on Antennas and Propagation, p.608-609.

Wang CX, Bian J, Sun J, et al., 2018. A survey of 5G channel measurements and models. *IEEE Commun Surv Tutor*, 20(4):3142-3168. https://doi.org/10.1109/COMST.2018.2862141

Wang CX, Lv Z, Gao XQ, et al., 2022. Pervasive wireless channel modeling theory and applications to 6G GBSMs for all frequency bands and all scenarios. *IEEE Trans Veh Technol*, 71(9):9159-9173. https://doi.org/10.1109/TVT.2022.3179695

Wang J, Wang CX, Huang J, et al., 2023. A novel THz massive MIMO beam domain channel model for 6G wireless communication systems. *IEEE Trans Veh Technol*, 72(8):9704-9719. https://doi.org/10.1109/TVT.2023.3257490

Wei L, Huang CW, Alexandropoulos GC, et al., 2022. Multi-user holographic MIMO surfaces: channel modeling and spectral efficiency analysis. *IEEE J Sel Top Signal Process*, 16(5):1112-1124. https://doi.org/10.1109/JSTSP.2022.3176140

Willhammar S, Flordelis J, van der Perre L, et al., 2018. Channel hardening in massive MIMO—a measurement based analysis. 19th Int Workshop on Signal Processing Advances in Wireless Communications, p.1-5. https://doi.org/10.1109/SPAWC.2018.8445925

Willhammar S, Flordelis J, van der Perre L, et al., 2020. Channel hardening in massive MIMO: model parameters and experimental assessment. *IEEE Open J Commun Soc*, 1:501-512. https://doi.org/10.1109/OJCOMS.2020.2987704

Wu SB, Wang CX, Aggoune EHM, et al., 2014. A non-stationary 3-D wideband twin-cluster model for 5G massive MIMO channels. *IEEE J Sel Areas Commun*, 32(6):1207-1218. https://doi.org/10.1109/JSAC.2014.2328131

Wu SB, Wang CX, Aggoune EHM, et al., 2015. A novel Kronecker-based stochastic model for massive MIMO channels. IEEE/CIC Int Conf on Communications in China, p.1-6. https://doi.org/10.1109/ICCChina.2015.7448642

Xu CP, Zhang JH, Zheng QF, et al., 2017. Measurement-based delay spread analysis of wideband massive MIMO system at 3.5 GHz. IEEE Int Conf on Computational Electromagnetics, p.246-248. https://doi.org/10.1109/COMPEM.2017.7912838

Yang B, Liang X, Liu SN, et al., 2023. Intelligent 6G wireless network with multi-dimensional information perception dimensional. *ZTE Commun*, 21(2):3-10. https://doi.org/10.12142/ZTECOM.202302002

Yang SJ, Lyu WT, Hu ZZ, et al., 2023. Channel estimation for near-field XL-RIS-aided mmWave hybrid beamforming architectures. *IEEE Trans Veh Technol*, 72(8):11029-11034. https://doi.org/10.1109/TVT.2023.3261340

Yang Y, Zheng Y, Wang CX, et al., 2022. Channel capacities of non-stationary 6G massive MIMO channels with mutual coupling verified by channel measurements. 33rd Annual Int Symp on Personal, Indoor and Mobile Radio Communications, p.1288-1293. https://doi.org/10.1109/PIMRC54779.2022.9977728

Yao JL, Ren HP, Liu Q, 2017. Massive MIMO channel modeling using map-based ray tracing method. 7th IEEE Int Symp on Microwave, Antenna, Propagation, and EMC Technologies, p.1-5. https://doi.org/10.1109/MAPE.2017.8250781

Yu H, Zhang JH, Zheng QF, et al., 2016. The rationality analysis of massive MIMO virtual measurement at 3.5 GHz. IEEE/CIC Int Conf on Communications in China, p.1-5. https://doi.org/10.1109/ICCChinaW.2016.7586715

Yuan Y, He RS, Ai B, et al., 2022. A 3D geometry-based THz channel model for 6G ultra massive MIMO systems. *IEEE Trans Veh Technol*, 71(3):2251-2266. https://doi.org/10.1109/TVT.2022.3143500

Yuan ZQ, Zhang JH, Ji YL, et al., 2023a. Spatial non-stationary near-field channel modeling and validation for massive MIMO systems. *IEEE Trans Antenn Propag*, 71(1):921-933. https://doi.org/10.1109/TAP.2022.3218759

Yuan ZQ, Zhang FC, Zhang YX, et al., 2023b. On phase mode selection in the frequency-invariant beamformer for near-field mmWave channel characterization. *IEEE Trans Antenn Propag*, 71(11):8975-8986. https://doi.org/10.1109/TAP.2023.3316791

Yuan ZQ, Zhang JH, Degli-Esposti V, et al., 2024. Efficient ray-tracing simulation for near-field spatial non-stationary mmWave massive MIMO channel and its experimental validation. *IEEE Trans Wirel Commun*,

23(8):8910-8923.
https://doi.org/10.1109/TWC.2024.3357071

Zhai M, Li JZ, Liang Y, et al., 2016. A novel coupling mode based 3D MIMO channel modeling and capacity analysis for 5G. IEEE Int Conf on Ubiquitous Wireless Broadband, p.1-4.
https://doi.org/10.1109/ICUWB.2016.7790499

Zhang JH, 2016. The interdisciplinary research of big data and wireless channel: a cluster-nuclei based channel model. *China Commun*, 13(S2):14-26.
https://doi.org/10.1109/CC.2016.7833457

Zhang JH, Zheng Z, Zhang YX, et al., 2018. 3D MIMO for 5G NR: several observations from 32 to massive 256 antennas based on channel measurement. *IEEE Commun Mag*, 56(3):62-70.
https://doi.org/10.1109/MCOM.2018.1700846

Zhang JH, Lin JX, Tang P, et al., 2023. Channel measurement, modeling, and simulation for 6G: a survey and tutorial. https://doi.org/10.48550/arXiv.2305.16616

Zhang JH, Lin JX, Tang P, et al., 2024a. Deterministic ray tracing: a promising approach to THz channel modeling in 6G deployment scenarios. *IEEE Commun Mag*, 62(2):48-54.
https://doi.org/10.1109/MCOM.001.2200486

Zhang JH, Miao HY, Tang P, et al., 2024b. New mid-band for 6G: several considerations from the channel propagation characteristics perspective. *IEEE Commun Mag*, early access. https://doi.org/10.1109/MCOM.001.2300708

Zhang P, Chen JQ, Yang XL, et al., 2018. Recent research on massive MIMO propagation channels: a survey. *IEEE Commun Mag*, 56(12):22-29.
https://doi.org/10.1109/MCOM.2018.1800196

Zhao YQ, Ke HQ, Xu W, et al., 2024. RIS-assisted cell-free MIMO: a survey. *ZTE Commun*, 22(1):77.
https://doi.org/10.12142/ZTECOM.202401009

Zheng Y, Wang CX, Yang RR, et al., 2023. Ultra-massive MIMO channel measurements at 5.3 GHz and a general 6G channel model. *IEEE Trans Veh Technol*, 72(1):20-34. https://doi.org/10.1109/TVT.2022.3205896

Zhi KD, Pan CH, Ren H, et al., 2024. Performance analysis and low-complexity design for XL-MIMO with near-field spatial non-stationarities. *IEEE J Sel Areas Commun*, 42(6):1656-1672.
https://doi.org/10.1109/JSAC.2024.3389128

Zhou ZH, Wang CX, Zhang L, et al., 2023. A novel SAGE algorithm for estimating parameters of wideband spatial nonstationary wireless channels with antenna polarization. *IEEE Trans Antenn Propag*, 71(9):7457-7472.
https://doi.org/10.1109/TAP.2023.3292508